# High fidelity simulations on the development of shock-induced hydrodynamic instability

Wednesday, 25th January 2023

**Satyvir Singh**

**Applied and Computational Mathematics (ACoM),**
**RWTH Aachen University, Germany**
*singh@acom.rwth-aachen.de*

# Outlines of the talk

- ❖ Research exposure and interest
- ❖ Introduction and motivation
- ❖ Mathematical formulation
- ❖ High-order numerical method
- ❖ Numerical results and discussion
- ❖ Concluding remarks and future study

# Research exposures

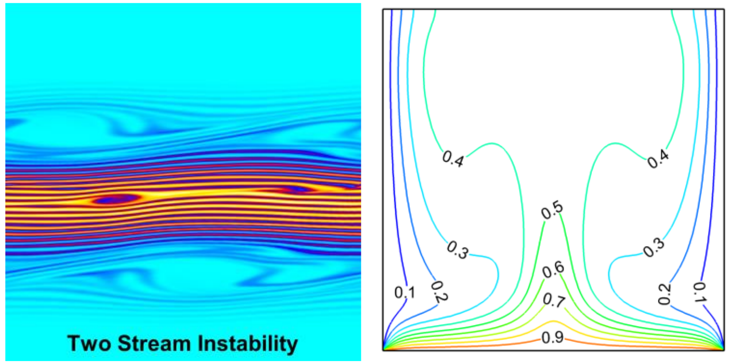


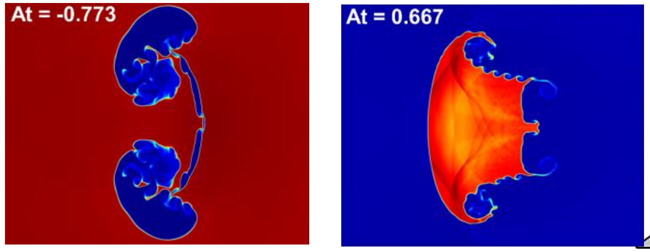


Singh, Phy. Fluids. (2022)

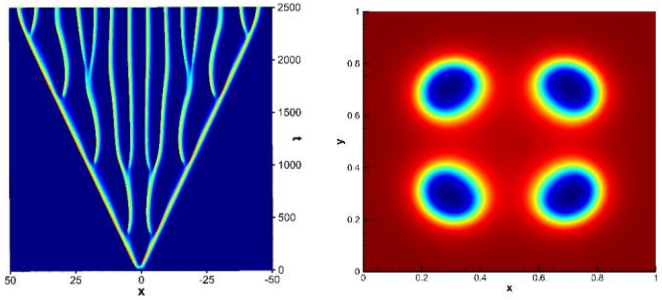

Singh, Appl. Math. Compt. (2023)

Plasma Physics, and Heat Convection - RWTH, Germany

Continuum-rarefied gas flows - GNU (South Korea)

Hydrodynamic instability and Turing pattern – NTU, Singapore

Boltzmann transport for ultrafast dynamics - NTU, Singapore

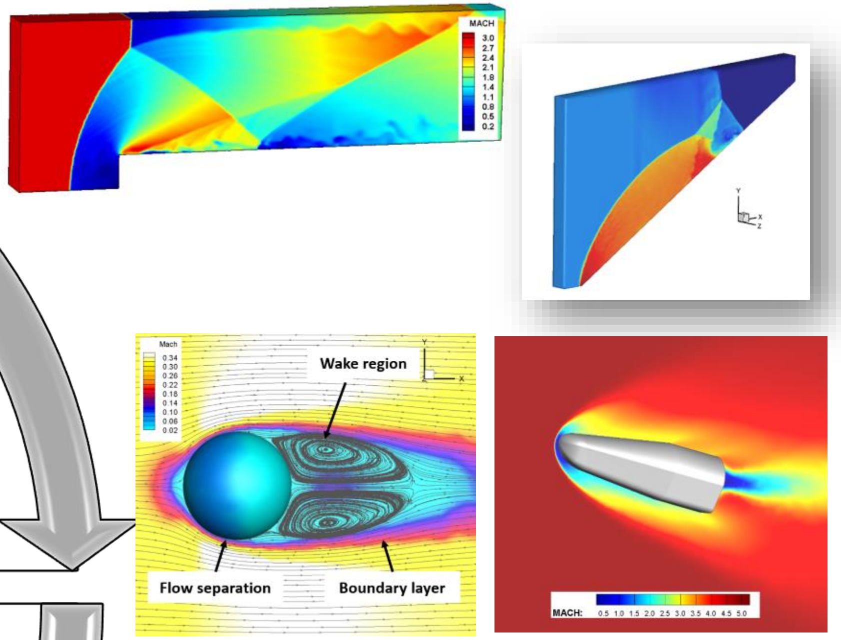


S. Singh *et.al.*, J. Comput. Phys. (2022)

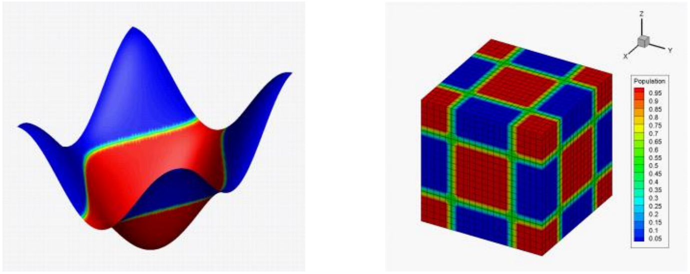

Singh and Battiato, Comput. Fluids. (2021)

# Research Interests

- High-order numerical methods – discontinuous Galerkin
- Kinetic theory for continuum-rarefied gas flows
- Physics of multi-components gas flows
- Shock-induced hydrodynamic instability
- Patter formations in biological process
- Heat and mass transfer
- Turbulent flows
- Maximum-Entropy moment methods for Vlasov system

# Introduction

- Hydrodynamic instability research determines whether a flow is stable or unstable, and if so, how these instabilities develop the turbulent mixing.
- There are **three primary hydrodynamic instabilities** in fluid dynamics.

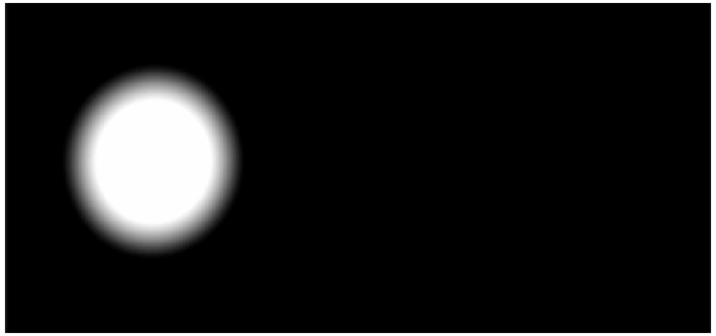

Richtmyer-Meshkov instability (RMI)

Kelvin-Helmholtz instability (KHI)

Rayleigh-Taylor instability (RTI)

- RMI is a **shock-induced hydrodynamic instability** that occurs in combination with the KHI when an initially perturbed interface separating by distinct fluid properties is accelerated by an incident shock wave.
- RMI can be considered as the impulsive limit of RTI, where primary perturbations expand across the interface and ultimately emerge into a turbulent fluid mixing as the uniform gravitational acceleration increases.

# Introduction

❖ In RMI, when an incident shock wave strikes on a bubble interface of density inhomogeneity, various complex wave patterns occur, and subsequent turbulent mixing generates along the gas interface due to the **baroclinic mechanism** ***i.e. misalignment between the density and pressure gradients***.

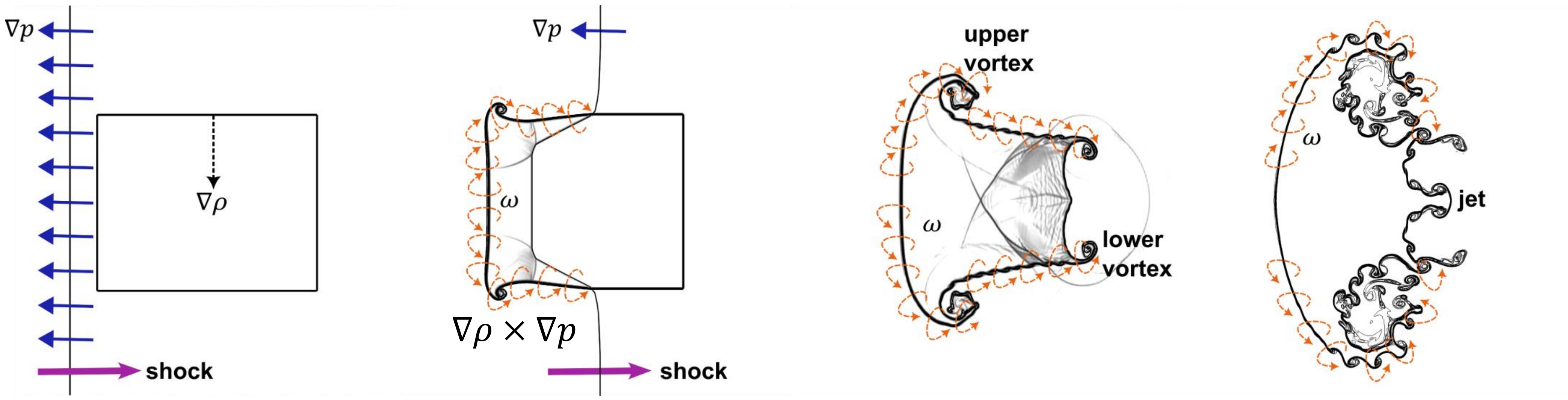


## Applications

- ❖ **Supersonic combustion in scramjet engines**
- ❖ **Explosive detonation**
- ❖ **Supernova explosions**
- ❖ **Inertial confinement fusion**
- ❖ **Medical shock wave Lithotripsy, and many more…….**

# Motivation

- ❖ **Shock-bubble interaction** is a basic and fundamental configuration in the studies of shock-induced hydrodynamic instability.
- ❖ For the development of shock-induced hydrodynamic instability on gas bubbles:
  - ✓ Mathematical Modeling for multi-component gas flows
  - ✓ Numerical method for simulations of multi-component gas flows
  - ✓ Validation of numerical solver
  - ✓ Physics of flow field etc.
- ❖ Few studies are available on the **shock-induced gas bubbles having polygonal interfaces** that provide good conditions for shock refraction physical phenomena.
- ❖ The thermal non-equilibrium effects, including bulk viscosity of diatomic and polyatomic gases on the flow morphology of shock-induced polygonal bubbles will be investigated.
- ❖ The effects of shock Mach number and aspect ratio on the shock-accelerated polygonal bubbles will be investigated.

# Mathematical formulation for shock-induced hydrodynamics instability

# Model 1: 2D compressible Euler equations for two-component gas flows

**The shock-induced hydrodynamic instability are basically simulated by solving the compressible multi-species flow model with a gas mixture.**

$$\frac{\partial}{\partial t}\begin{bmatrix}\rho\\ \rho u\\ \rho v\\ \rho E\\ \rho\phi\end{bmatrix}+\frac{\partial}{\partial x}\begin{bmatrix}\rho u\\ \rho u^2+p\\ \rho uv\\ (\rho E+p)u\\ \rho\phi u\end{bmatrix}+\frac{\partial}{\partial y}\begin{bmatrix}\rho v\\ \rho uv\\ \rho v^2+p\\ (\rho E+p)v\\ \rho\phi v\end{bmatrix}=\begin{bmatrix}0\\0\\0\\0\\0\end{bmatrix}$$

$\rho$ : mass density
$u, v$ : components of velocity vector
$p$ : pressure
$E$ : total energy
$\phi$ : mass fraction

**Total energy is calculated as**

$$\rho E=\frac{p}{\gamma_{mix}-1}+\frac{1}{2}\rho\left(u^2+v^2\right)$$

where

$$\gamma_{mix}=\frac{C_{p_1}\phi_1+C_{p_2}\phi_2}{C_{v_1}\phi_1+C_{v_2}\phi_2}$$

$\phi_1$ : mass fraction for first component
$\phi_2=1-\phi_1$ : mass fraction for second component

Shankar et al., Physics of Fluids, 23, 024102 (2011)

# Model 2: 2D compressible Navier-Fourier equation for single gas flows

- Interestingly, it has been found in the previous research works of Picone and Boris (JFM,1988) Samtaney and Zabusky (JFM, 1994), Quirk and Karni (JFM, 1996) that ***the different values of specific heat capacities values for each gas do not affect the details of the vorticity generation qualitatively, particularly the creation of large-scale structures.***

- This model can be configured as an unsteady compressible laminar flow that assumes a **single-component perfect gas** with a specific heat ratio.

# Model 2: 2D compressible Navier-Fourier equation for single gas flows

**Compressible Navier-Stokes-Fourier (NSF) equations**

$$\frac{\partial}{\partial t}\begin{bmatrix}\rho\\ \rho\mathbf{u}\\ \rho E\end{bmatrix}+\nabla\cdot\begin{bmatrix}\rho\mathbf{u}\\ \rho\mathbf{u}\mathbf{u}+p\mathbf{I}\\ (\rho E+p)\mathbf{u}\end{bmatrix}+\nabla\cdot\begin{bmatrix}0\\ \mathbf{\Pi}\\ \mathbf{\Pi}\cdot\mathbf{u}+\mathbf{Q}\end{bmatrix}=\begin{bmatrix}0\\0\\0\end{bmatrix}$$

$\mathbf{u}$ : velocity vector

$\mathbf{\Pi}$ : viscous stress

$\mathbf{Q}$ : heat flux

$$\boxed{\frac{\partial \mathbf{U}}{\partial \mathrm{t}}+\nabla\cdot\mathbf{F}_{\mathrm{inv}}(\mathbf{U})+\nabla\cdot\mathbf{F}_{\mathrm{vis}}(\mathbf{U},\nabla\mathbf{U})=0}$$

**NSF equation is considered as *de facto* mathematical equation for all possible flow**

**Stokes' hypothesis (1845):**

$$\boxed{\mu_b\approx\lambda+\frac{2}{3}\mu=0,\ \text{equivalently,}\ \ \lambda=-\frac{2}{3}\mu,}$$

$\mu_b$ : bulk visocsity

$\mu$ : first coefficient of visocsity (shear viscosity)

$\lambda$ : second coefficient of visocsity

**This assumption is valid only for monatomic gas and at thermal equilibrium condition.**

# Model 2: 2D compressible Navier-Fourier equation for single gas flows

**In non-monatomic gases,**

- **Rotational and vibrational modes are closely related to thermal non-equilibrium.**
- **Rotational nonequilibrium effects are easily excited  at room temperature.**
- **Vibrational non-equilibrium effects become relevant when the temperature is greater than 1000 K**

**In this study,**

- **Considered room temperature (~ 300 K)**
- **Neglecting Vibrational non-equilibrium effects**
- **Rotational thermal non-equilibrium effects are accounted by introducing with excess normal stress**

$$\boxed{\Delta = -\mu_b \nabla \cdot \mathbf{u}}$$

where $\mu_b = \text{bulk visocsity} = f_b \cdot \mu$

$\mu = \text{first coefficient of visocsity (shear viscosity)}$

$\nabla \cdot \mathbf{u} = \text{dilatational term}$

# Model 2: 2D compressible Navier-Fourier equation for single gas flows

**In monatomic gases,**

$$\boxed{\Delta = 0 \text{ equivalently, } \nabla \cdot \mathbf{u} = 0}$$

For non-monatomic gases -- nitrogen (air), methane and $CO_2$,

dilatational term, $\nabla \cdot \mathbf{u}$ plays a significant role in compressible flow.

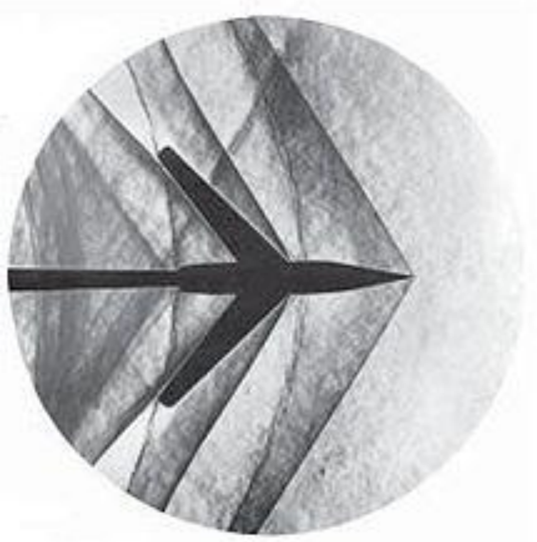

Inner structure of strong shock waves

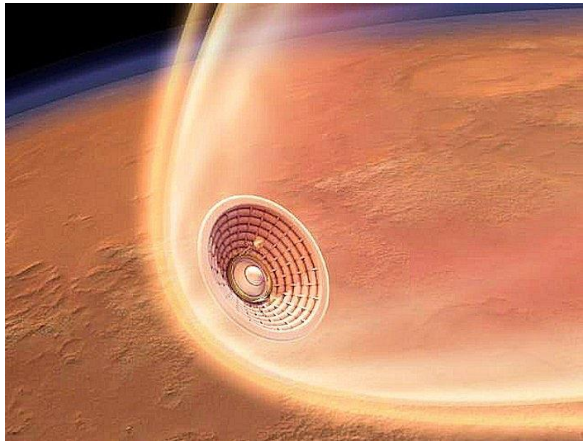

$\mu_{bulk} \approx 2000\mu$

Hypersonic entry into Mars and Venus atmosphere

| | |
|---|---|
| Argon gas: | $\mu_b \approx 0,$ |
| Nitrogen gas: | $\mu_b \approx 0.8\mu,$ |
| Methane gas: | $\mu_b \approx 1.33\mu,$ |
| Carbon dioxide gas: | $\mu_b \approx 2000\mu.$ |

# Model 2: 2D compressible Navier-Fourier equation for single gas flows

**For non-monatomic gases, compressible Navier-Fourier (NF) equations**

$$\frac{\partial}{\partial t}\begin{bmatrix} \rho \\ \rho\mathbf{u} \\ \rho E \end{bmatrix} + \nabla\cdot\begin{bmatrix} \rho\mathbf{u} \\ \rho\mathbf{u}\mathbf{u} + p\mathbf{I} \\ (\rho E + p)\mathbf{u} \end{bmatrix} + \nabla\cdot\begin{bmatrix} 0 \\ \mathbf{\Pi} + \Delta\mathbf{I} \\ (\mathbf{\Pi} + \Delta\mathbf{I})\mathbf{u} + \mathbf{Q} \end{bmatrix} = \begin{bmatrix} 0 \\ 0 \\ 0 \end{bmatrix}$$

$\mathbf{\Pi}$ : viscous stress,

$\Delta$ : excess normal stress,

$\mathbf{Q}$ : heat flux.

**where**

$$\boxed{\mathbf{\Pi} = 2\mu[\nabla\mathbf{u}]^{(2)}, \quad \Delta = -\mu_b \nabla\cdot\mathbf{u}, \quad \mathbf{Q} = k\nabla T}$$

**Chapman-Enskog linear transport coefficients**

$$\boxed{\mu = \left(\frac{T}{T_{ref}}\right)^{s+1}, \quad \mu_b = f_b\mu, \quad k = \left(\frac{T}{T_{ref}}\right)^{s}}$$

$s \rightarrow$ the index of the inverse power laws of gas molecules

$$\boxed{s = \frac{1}{2} + \frac{1}{\upsilon - 1}}$$

$\upsilon$ : exponent of the inverse power laws for the gas-particle interaction potentials

# High-order numerical method

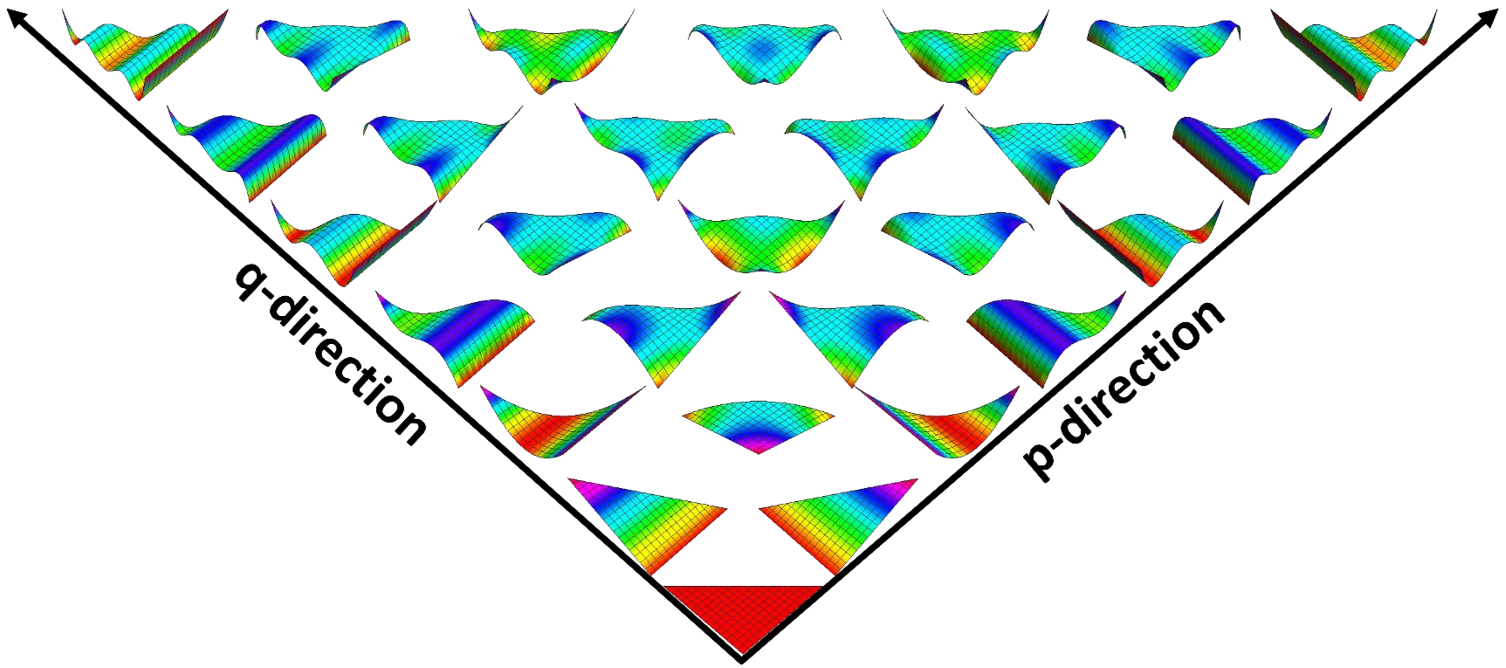

# High-order Numerical Method for Modern CFD

## Which kind of numerical approach can be suitable for solving highly non-linear system ?

**Numerical Methods for Modern CFD**

- **Finite Difference Method**
- **Finite Volume Method**
- **Finite Element Method**
- **High-order Spectral methods**
  - **Spectral Difference (SD)**
  - **Spectral Volume (SV)**
  - **Discontinuous Galerkin (DG)**
    - **Modal DG**
    - **Nodal DG**

**High order methods are needed for solving challenging problems, (such as *aeroacoustics*, turbulent flow)**

- *Steady and unsteady*
- *Complex geometries*
- *Multi-physics phenomena*
- *Multi-scales problem in space and time*

# High-order Numerical Method for Modern CFD

## Finite Difference Methods

**Advantages**

- Easy to implement
- Easy to make high-order

**Disadvantages**

- Applicable only for structured meshes

## Finite Volume Methods

**Advantages**

- Naturally conservative (captures discontinuity in the flow field)
- Applicable on any type of meshes – structured, unstructured

**Disadvantages**

- Difficult to devise stable higher order scheme (need **ENO-WENO** schemes etc.)

## Finite Element Methods

**Advantages**

- Can be any order of accuracy
- Applicable on any type of meshes – structured, unstructured

**Disadvantages**

- Not naturally conservative

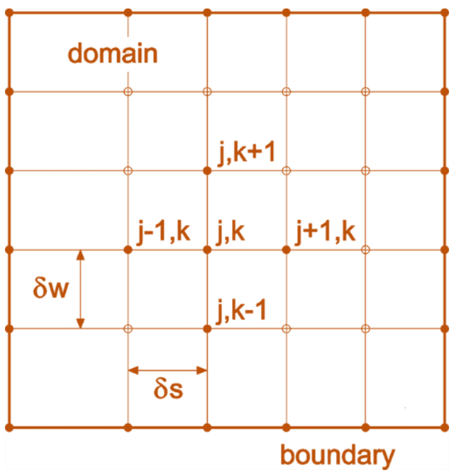


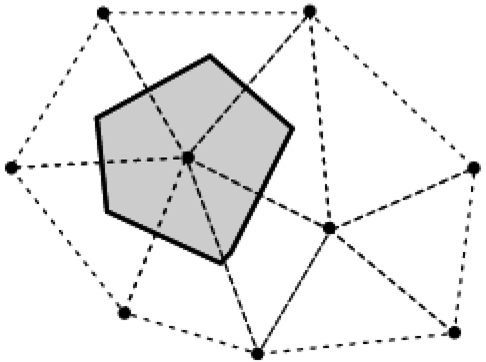

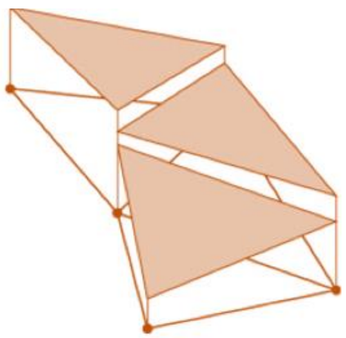

# High-order Discontinuous Galerkin Method

| | FVM | FDM | FEM | DG |
|---|---|---|---|---|
| High-order/Low dispersion | ✗ | ✓ | ✓ | ✓ |
| Unstructured meshes | ✓ | ✗ | ✓ | ✓ |
| Stability for convervation laws | ✓ | ✓ | ✗ | ✓ |

**DG method = FV method + FE method**

## Advantages

- Strong mathematical supports
- *hp*–adaptivity (geometric and order-accuracy flexibility)
- Provide high-order accurate solution
- Easy to handle arbitrary grid (structured and unstructured)
- Highly parallel efficiency due to local nature
- Possible to solve any PDE system (Hyperbolics, Parabolic, Elliptic)

## Drawbacks

- High order methods are not necessary, for most of the engineering applications.
- Extra efforts are needed for solving viscous dominant flows and elliptic PDEs
- Extra efforts are needed for simulation of the complex geometries with curve boundaries
- Extra efforts for limiters in case of discontinuous problems
- Too expensive

# Mixed-type discontinuous Galerkin formulation

1D Viscous Burger's equation : $\frac{\partial u}{\partial t}+\frac{\partial}{\partial x}\left(\frac{1}{2}u^2\right)-\frac{\partial}{\partial x}\left(\mu\frac{\partial u}{\partial x}\right)=0,$

auxiliary variable

$$\begin{cases}\Theta=\mu\frac{\partial u}{\partial x},\\ \frac{\partial u}{\partial t}+\frac{\partial}{\partial x}\left(\frac{1}{2}u^2-\Theta\right)=0.\end{cases}$$

Coupled first – order system for u and $\Theta$

Conservation laws with source term: $\boxed{\frac{\partial \mathbf{U}}{\partial t}+\nabla\cdot\mathbf{F}_{inv}(\mathbf{U})+\nabla\cdot\mathbf{F}_{vis}(\mathbf{U},\nabla\mathbf{U})=0}$

$\mathbf{U}$ – conservative variables

$\mathbf{F}_{inv}(\mathbf{U})$ – inviscid flux function

$\mathbf{F}_{vis}(\mathbf{U},\nabla\mathbf{U})$ – viscous flux function

$S(\mathbf{U})$ – source term

Mixed form of Conservation laws: $\boxed{\begin{cases}\Theta=\nabla\mathbf{U},\\ \partial_t\mathbf{U}+\nabla\mathbf{F}_{inv}(\mathbf{U})+\nabla\mathbf{F}_{vis}(\mathbf{U},\Theta)=\mathbf{S}(\mathbf{U})\end{cases}}$

Coupled first – order system for $\mathbf{U}$ and $\Theta$

**Source** : **J.N. Reddy**, ***An Introduction of the Finite Element Method***, **Tata McGraw-Hill, 2012**

# Computational domain: decomposition and transformation

Computational domain is tessellated into a collection of non-overlapping elements

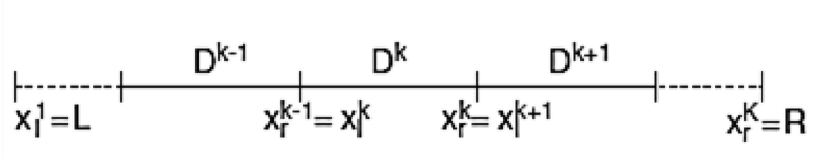


$$\Omega \simeq \Omega_h = \bigcup_{k=1}^{K} D^k,$$

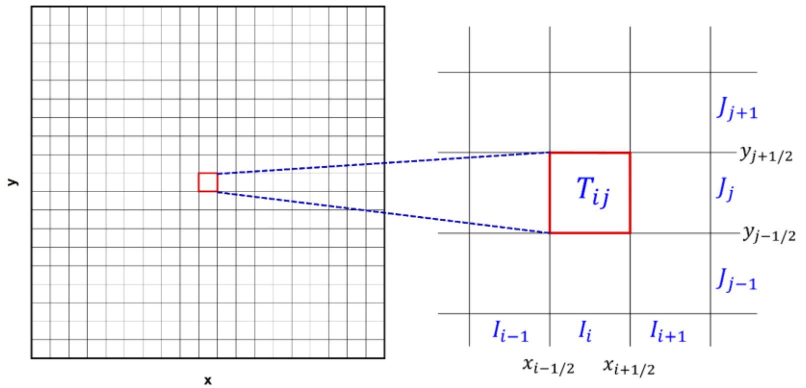


Elemental transformation according to numerical integration rule

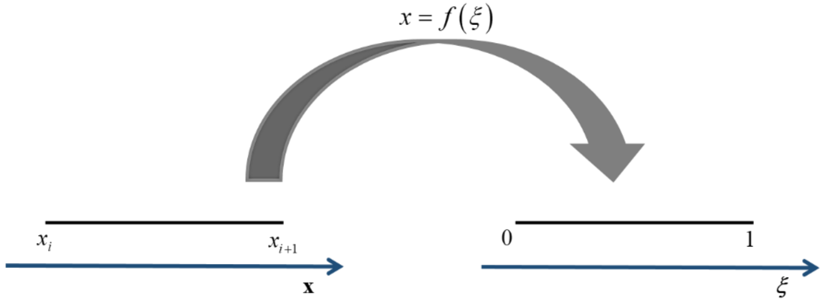


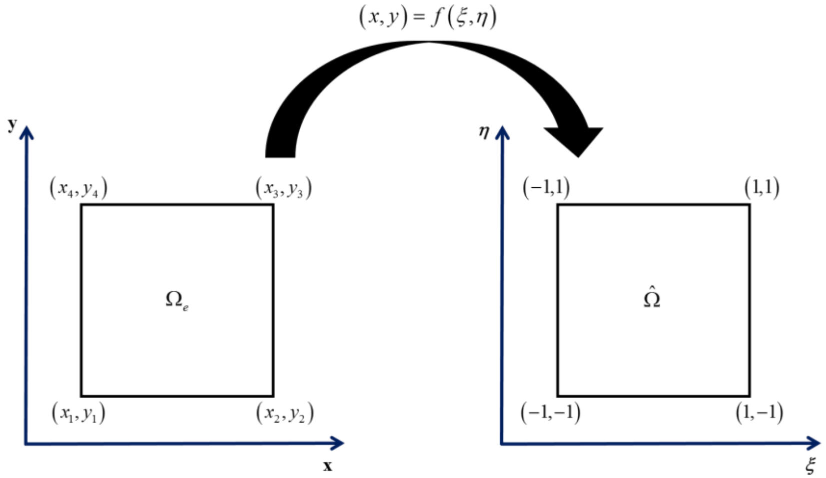

# Mixed-type discontinuous Galerkin formulation

Conservation laws with source term: $\frac{\partial \mathbf{U}}{\partial t} + \nabla \cdot \mathbf{F}_{\text{inv}}(\mathbf{U}) + \nabla \cdot \mathbf{F}_{\text{vis}}(\mathbf{U}, \nabla \mathbf{U}) = 0$

**Mixed form of conservation laws :** $\boxed{\begin{cases} \Theta - \nabla \mathbf{U} = 0 \\ \partial_t \mathbf{U} + \nabla \mathbf{F}_{\text{inv}}(\mathbf{U}) + \nabla \mathbf{F}_{\text{vis}}(\mathbf{U}, \Theta) = 0 \end{cases}}$

Multiplying by a test function $q(\boldsymbol{x})$ and integrate over element

$$\begin{cases} \int_E \Theta q(\mathbf{x}) \, \mathrm{d}\Omega - \int_E \nabla \mathbf{U} \cdot q(\mathbf{x}) \, \mathrm{d}\Omega = 0, \\ \int_E \frac{\partial \mathbf{U}}{\partial t} q(\mathbf{x}) \, \mathrm{d}\Omega + \int_E \left( \nabla \mathbf{F}_{\text{inv}}(\mathbf{U}) + \nabla \mathbf{F}_{\text{vis}}(\mathbf{U}, \Theta) \right) \cdot q(\mathbf{x}) \, \mathrm{d}\Omega = 0 \end{cases}$$

**Using integration by parts and Green-Gauss divergence theorem:**

$$\begin{cases} \int_E \Theta q \, \mathrm{d}\Omega + \int_E \nabla q \, \mathbf{U} \, \mathrm{d}\Omega - \oint_{\partial E} \mathbf{U} \cdot \hat{\mathrm{n}} \cdot q \, \mathrm{d}\sigma = 0, \\ \int_E \frac{\partial \mathbf{U}}{\partial t} q \, \mathrm{d}\Omega + \int_E \left( \mathbf{F}_{\text{inv}}(\mathbf{U}) + \mathbf{F}_{\text{vis}}(\mathbf{U}, \mathbf{S}) \right) \nabla q \, \mathrm{d}\Omega - \oint_{\partial E} \left( \mathbf{F}_{\text{inv}}(\mathbf{U}) + \mathbf{F}_{\text{vis}}(\mathbf{U}, \mathbf{S}) \right) \cdot \hat{\mathrm{n}} \cdot q \, \mathrm{d}\sigma = 0. \end{cases}$$

# Mixed-type discontinuous Galerkin formulation

**FEM approach : Galerkin formulation**
**(high-order flexibility)**

test function : $q(\mathbf{x}) = \varphi_l(\boldsymbol{\xi}(\mathbf{x}))$

conservative variables : $\mathbf{U} \approx U_h = \sum_{l=1}^{N_k} \hat{u}_l(t)\varphi_l(\boldsymbol{\xi}(\mathbf{x}))$

auxiliary variable : $\Theta \approx \Theta_h = \sum_{l=1}^{N_k} \hat{s}_l(t)\varphi_l(\boldsymbol{\xi}(\mathbf{x}))$

where $N_k$ = number of basis function for the polynomial function $P^k$,

$\varphi_l(\boldsymbol{\xi}(\mathbf{x}))$ = basis function

**FVM approach: flux reconstruction**
**(Numerical fluxes)**

$$\mathbf{U}\cdot\hat{\mathrm{n}} \approx \hat{\mathrm{H}}_{aux}\left(\mathbf{U}^+, \mathbf{U}^-\right)$$

$$\mathbf{F}_{\mathrm{inv}}(\mathbf{U})\cdot\hat{\mathrm{n}} \approx \hat{\mathrm{H}}_{inv}(\mathbf{U}^+, \mathbf{U}^-)$$

$$\mathbf{F}_{\mathrm{vis}}(\mathbf{U},\mathbf{S})\cdot\hat{\mathrm{n}} \approx \hat{\mathrm{H}}_{vis}(\mathbf{U}^+, \mathbf{S}^-, \mathbf{U}^-, \mathbf{S}^-)$$

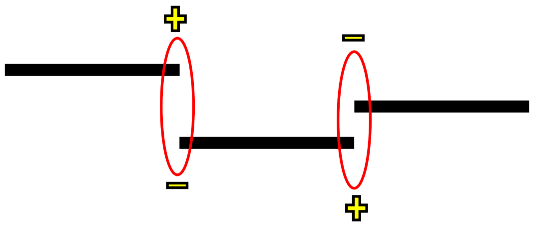

- **Consistency condition** : $\mathrm{H}(u,u) = f(u)$
- **Continuity condition** : $\mathrm{H}(u_L, u_R)$ is Lipschitz continous for $u_L$ and $u_R$
- **Monotonicity condition** : $\mathrm{H}(u_L, u_R)$ is $\mathrm{H}(\uparrow,\downarrow)$non-dereasing function of $u_L$, and non-increasing function of $u_R$.

# Weak formulation of mixed-type DG spatial discretization

$$\begin{cases} \int_E \left( \sum_{l=1}^{N_k} \hat{s}_l(t)\varphi_l(\xi(\mathbf{x})) \right) \varphi_m(\xi(\mathbf{x}))\,\mathrm{d}\Omega + \int_E \nabla\varphi_l(\xi(\mathbf{x}))\,\mathbf{U}\,\mathrm{d}\Omega - \oint_{\partial E} \hat{\mathrm{H}}_{aux}\cdot\varphi_l(\xi(\mathbf{x}))\,\mathrm{d}\sigma = 0, \\ \int_E \frac{\partial}{\partial t}\left( \sum_{l=1}^{N_k} \hat{u}_l(t)\varphi_l(\xi(\mathbf{x})) \right) \varphi_m(\xi(\mathbf{x}))\,\mathrm{d}\Omega + \int_E \mathbf{F}_{\mathrm{inv}}\,\nabla\varphi_l(\xi(\mathbf{x}))\,\mathrm{d}\Omega - \oint_{\partial E} \hat{\mathrm{H}}_{inv}\cdot\varphi_l(\xi(\mathbf{x}))\,\mathrm{d}\sigma \\ \qquad + \int_E \mathbf{F}_{\mathrm{vis}}\,\nabla\varphi_l(\xi(\mathbf{x}))\,\mathrm{d}\Omega - \oint_{\partial E} \hat{\mathrm{H}}_{vis}\cdot\varphi_l(\xi(\mathbf{x}))\,\mathrm{d}\sigma = 0 \end{cases}$$

$$\Downarrow$$

$$\begin{cases} \hat{s}_l(t)\int_E \varphi_l(\xi(\mathbf{x}))\varphi_m(\xi(\mathbf{x}))\,\mathrm{d}\Omega + \int_E \nabla\varphi_l(\xi(\mathbf{x}))\,\mathbf{U}\,\mathrm{d}\Omega - \oint_{\partial E} \hat{\mathrm{H}}_{aux}\cdot\varphi_l(\xi(\mathbf{x}))\,\mathrm{d}\sigma = 0, \\ \frac{\partial \hat{u}_l(t)}{\partial t} \boxed{\int_E \varphi_l(\xi(\mathbf{x}))\varphi_m(\xi(\mathbf{x}))\,\mathrm{d}\Omega} + \boxed{\int_E \mathbf{F}_{\mathrm{inv}}(U_h)\nabla\varphi_l(\xi(\mathbf{x}))\,\mathrm{d}\Omega} - \boxed{\oint_{\partial E} \hat{\mathrm{H}}_{inv}(\mathbf{U})\cdot\varphi_l(\xi(\mathbf{x}))\,\mathrm{d}\sigma} \\ \qquad + \int_E \mathbf{F}_{\mathrm{vis}}(\mathbf{U},\mathbf{S})\nabla\varphi_l(\xi(\mathbf{x}))\,\mathrm{d}\Omega - \oint_{\partial E} \hat{\mathrm{H}}_{vis}(\mathbf{U},\mathbf{S})\cdot\varphi_l(\xi(\mathbf{x}))\,\mathrm{d}\sigma = 0 \end{cases}$$

Mass matrix

Volume integration

Surface integration

# Temporal discretization

**Semi-discrete form of ordinary differential equation**

$$\boxed{\mathbf{M}\frac{\partial U_h}{\partial t} = \mathbf{L}\left(U_h\right)}$$

$$\mathbf{M} = \text{ orthogonal mass matrix}$$

$$\mathbf{L}\left(U_h\right) = \text{ residual function}$$

$$\mathbf{M} = \begin{cases} \int_{I_n} \varphi_i\,\varphi_j dk = C_{ij}, & \text{if } i = j \\ \int_{I_n} \varphi_i\,\varphi_j dk = 0, & \text{if } i \neq j \end{cases}$$

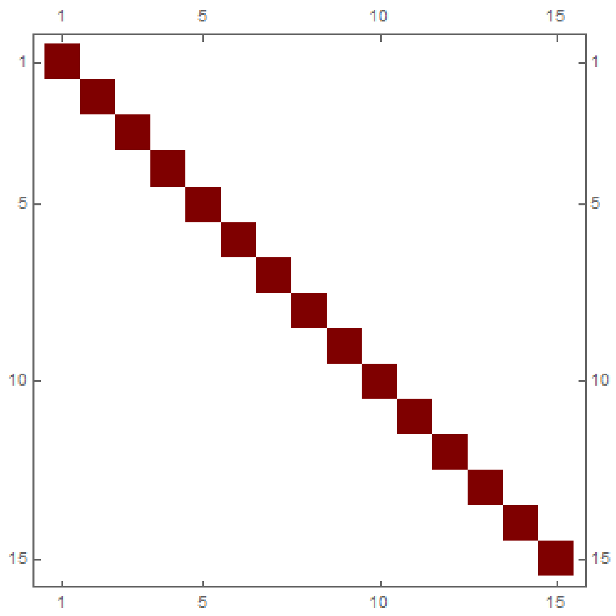


Orthogonal Mass matrix

**Explicit third-order TVD Runge-Kutta scheme**

$$U_h^{(1)} = U_h^n + \Delta t\,\mathbf{M}^{-1}\mathbf{L}\left(U_h^n\right)$$

$$U_h^{(2)} = \frac{3}{4}U_h^n + \frac{1}{4}U_h^{(1)} + \frac{1}{4}\Delta t\,\mathbf{M}^{-1}\mathbf{L}\left(U_h^{(1)}\right)$$

$$U_h^{n+1} = \frac{1}{3}U_h^n + \frac{2}{3}U_h^{(2)} + \frac{2}{3}\Delta t\,\mathbf{M}^{-1}\mathbf{L}\left(U_h^{(2)}\right),$$

# Basis (polynomial) functions

**Choosing an appropriate basis and test functions**

**Galerkin method:** Test function = basis function

Basis Family
- Lagrange
- Legendre
  - Dubiner
  - Proriol
  - Koornwinder
- Chebychev
- Fourier

**Basis functions**

| Orthogonal Basis functions | Non-orthogonal Basis functions |
|---|---|
| Modal Basis functions | Nodal Basis functions |
| Based on Legendre polynomial | Based on Lagrangian polynomial |
| $u_h(x,t)=\sum_{k=0}^{N_p}\hat{u}^k(t)\hat{\varphi}^k(x)$ | $u_h(x,t)=\sum_{k=0}^{N_p}u^k(x,t)\hat{l}^k(x)$ |

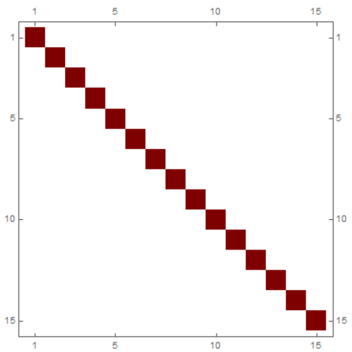

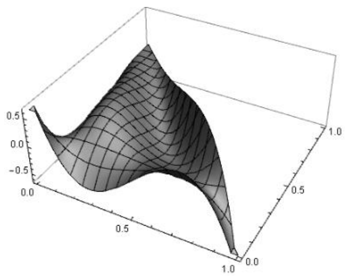

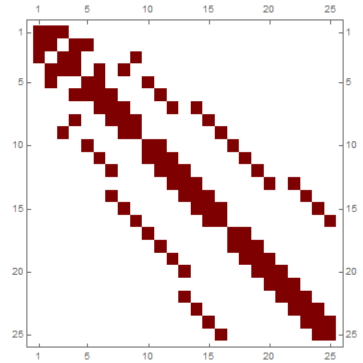

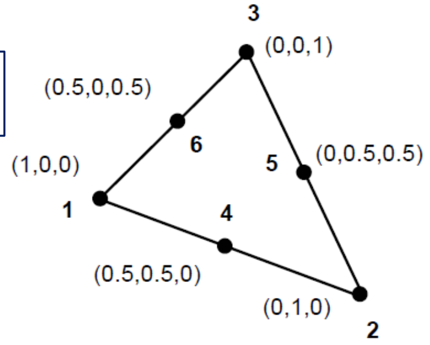

# Summary of present numerical scheme

- ❖ Computational domain decomposition with uniform rectangular meshes
- ❖ Hierarchical basis function based on Legendre polynomials
- ❖ Lax-Friedriches, Roe and HLLC schemes for inviscid flux term
- ❖ Alternating (Local DG) scheme for viscous and auxiliary flux terms
- ❖ Gauss-Legendre quadrature rule for surface and volume numerical integrations
- ❖ 3$^{rd}$-order TVD Runge-Kutta scheme for temporal integration
- ❖ A high-order moment limiter proposed by Krivodonova is used for controlling artificial oscillations

# Numerical Results

# Order accuracy test of present DG scheme

**A smooth 1D density wave propagation problem with initial condition:**

$$\left.\begin{aligned} u(x,0) &= 1.0 \\ \rho(x,0) &= 1.0 + 0.2\sin(\pi x) \\ p(x,0) &= 1.0 \end{aligned}\right\} \quad \forall x \in [0,6],$$

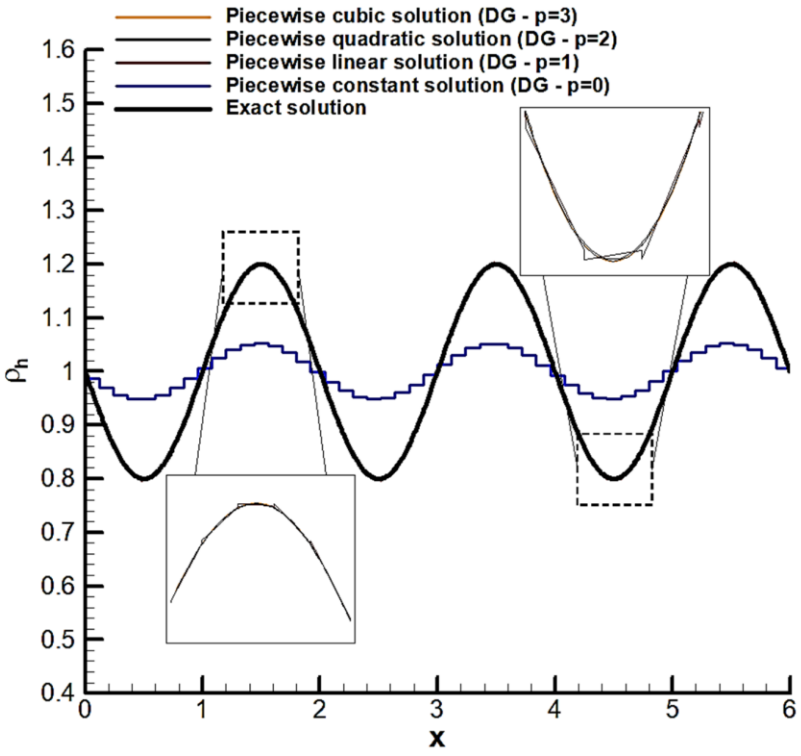


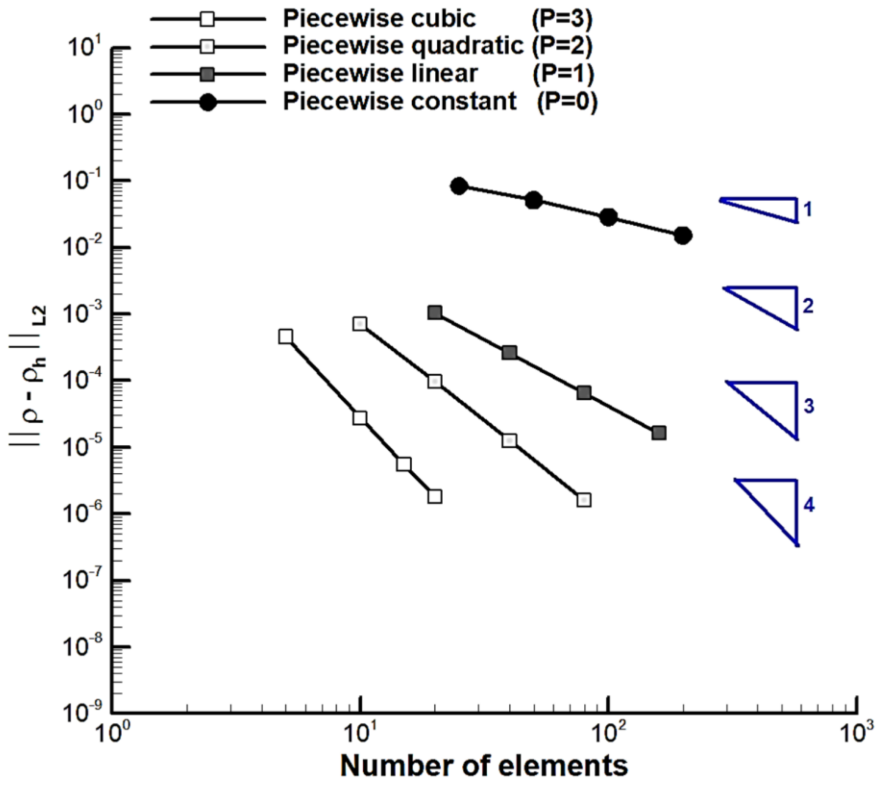


Achieved the desired order of accuracy ($p$+1)

# 1D–Riemann problem: Sod shock tube

$$\frac{\partial}{\partial t}\begin{bmatrix}\rho \\ \rho u \\ \rho E \\ \rho\phi\end{bmatrix}+\frac{\partial}{\partial x}\begin{bmatrix}\rho u \\ u^2+p \\ (\rho E+p)u \\ \rho\phi u\end{bmatrix}=\begin{bmatrix}0\\0\\0\\0\end{bmatrix}$$

**Initial condition**

$$(\rho,u,p,\gamma)=\begin{cases}(1.0,0.0,1.0,1.4), & \text{if } x\le 0.5,\\ (0.125,0,0.1,1.6) & \text{if } x>0.5\end{cases}$$

- **Final time = 0.25 sec.**
- **Discontinuity position, *x*=0.5**
- **3rd-order DG scheme**

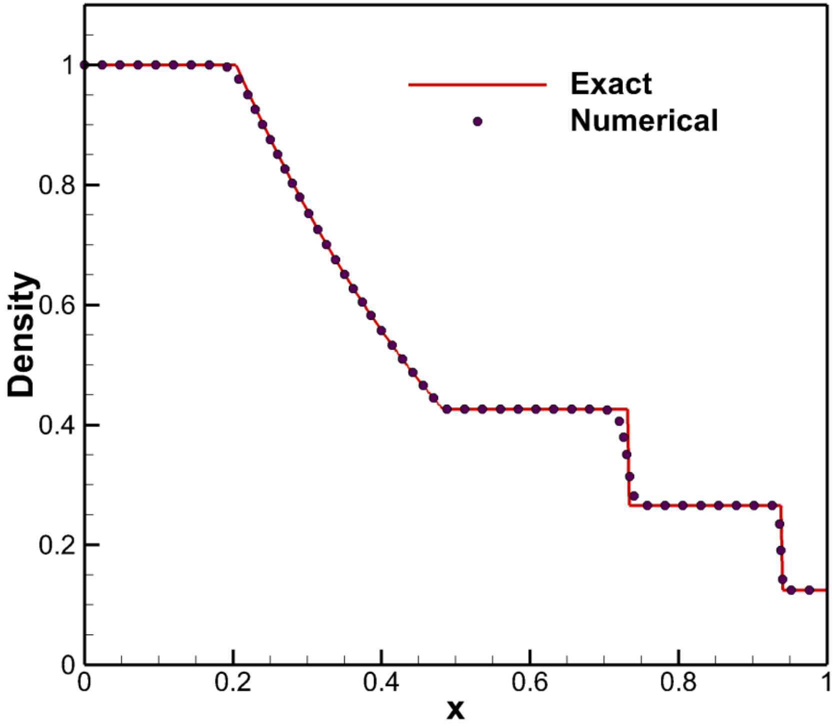


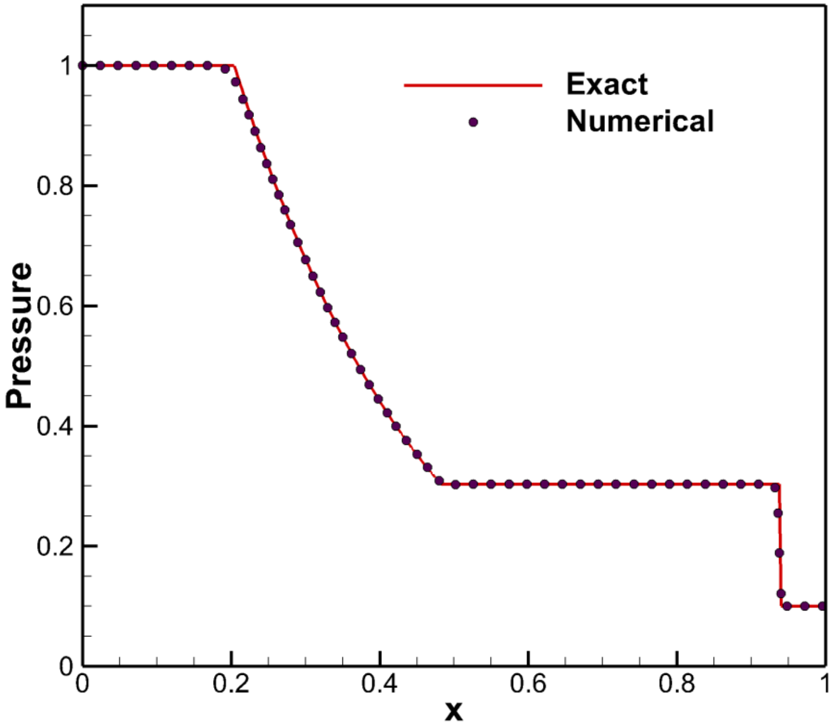


**Singh and Torrilhon, Physics of Fluids, 35, 012117 (2023)**

# 1D stiff shock structure problem

$$\frac{\partial}{\partial t}\begin{bmatrix}\rho\\ \rho u\\ \rho E\end{bmatrix}+\frac{\partial}{\partial x}\begin{bmatrix}\rho u\\ \rho u^2+p\\ (\rho E+p)u\end{bmatrix}=\begin{bmatrix}0\\ \mu u_{xx}\\ \mu u u_{xx}+\kappa T_x\end{bmatrix}$$

- **Argon gas**
- **3rd-order DG scheme**

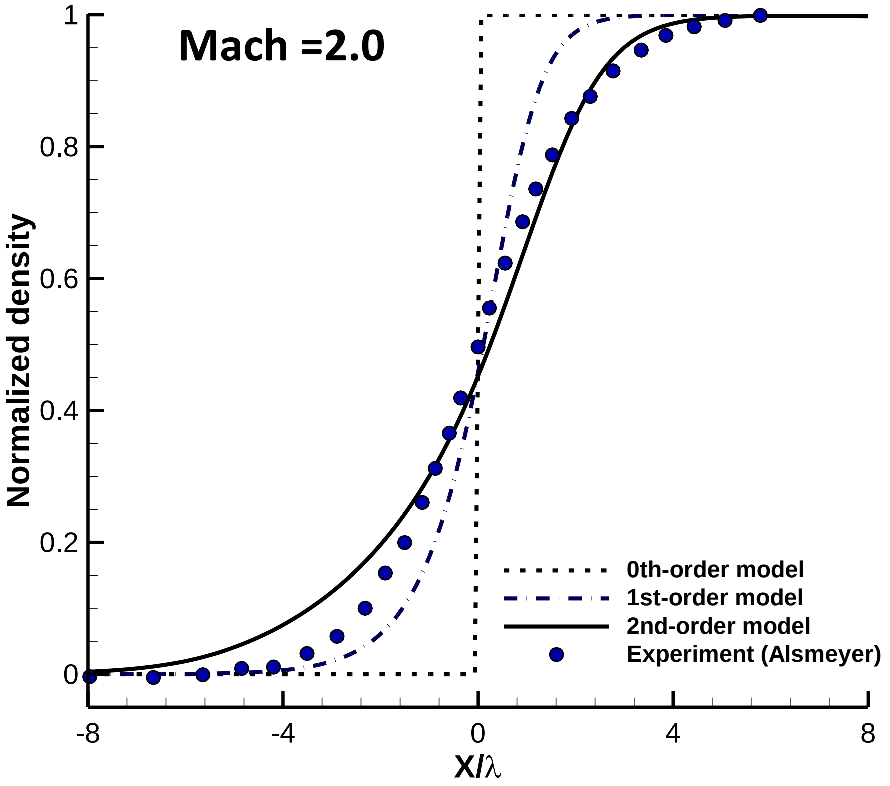


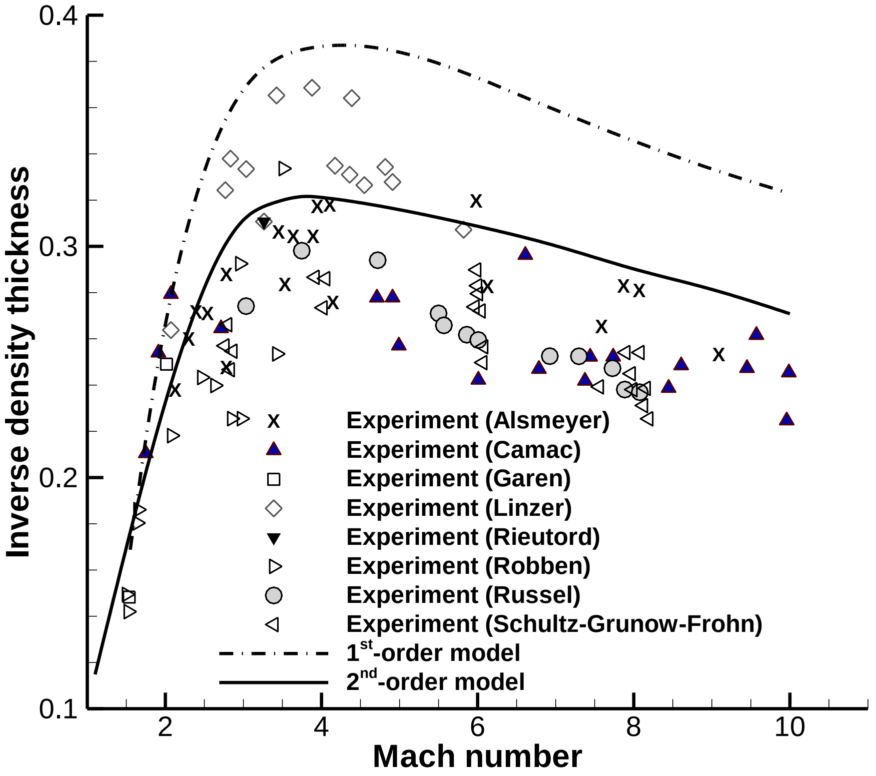


Singh et al., Journal of Computational Physics, 457, 111052 (2022)

# 2D shock-cylindrical bubble interaction

Shock Mach number =1.22

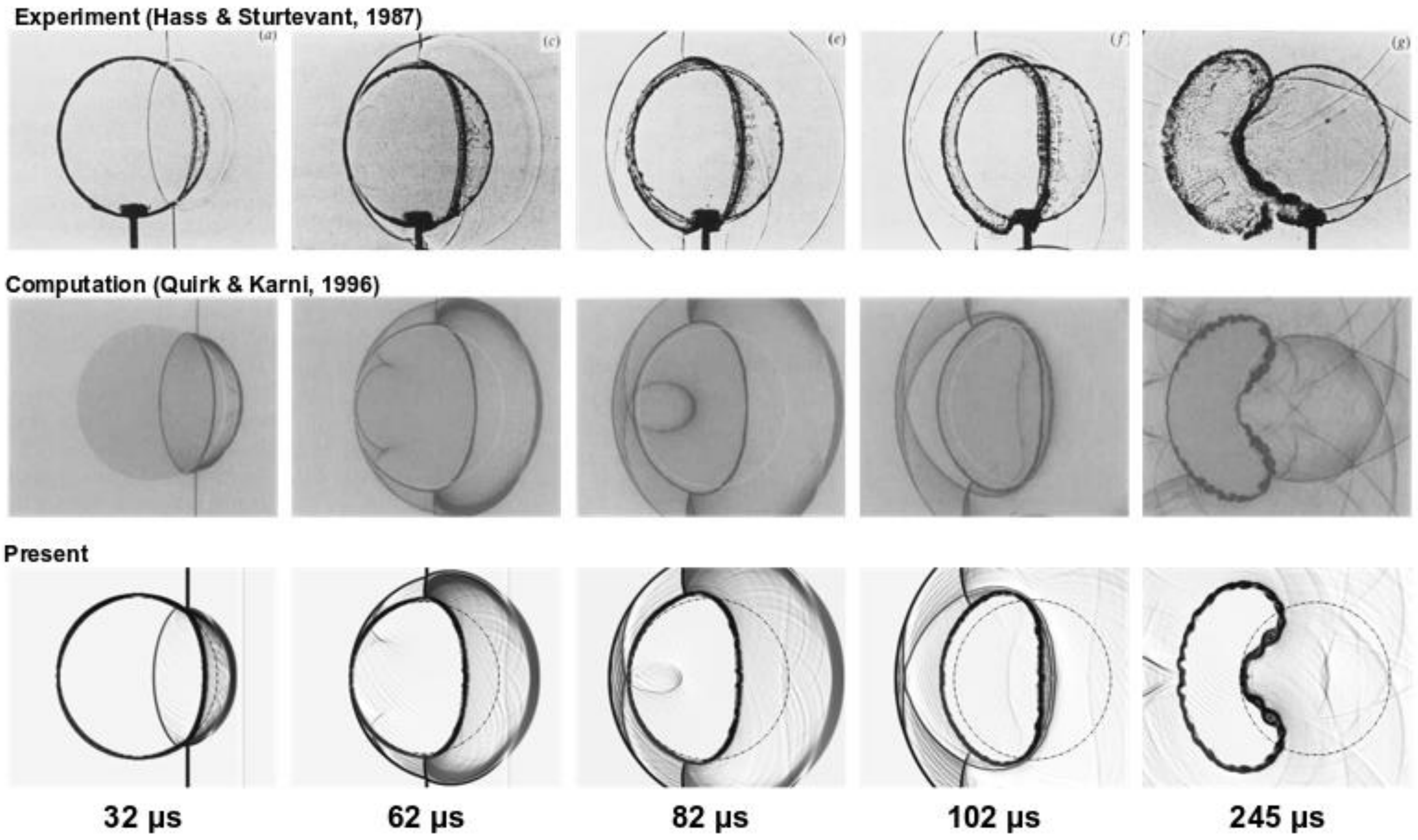


Numerical schlieren images

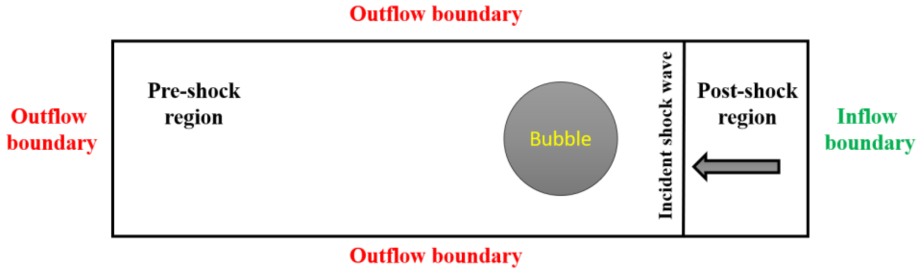


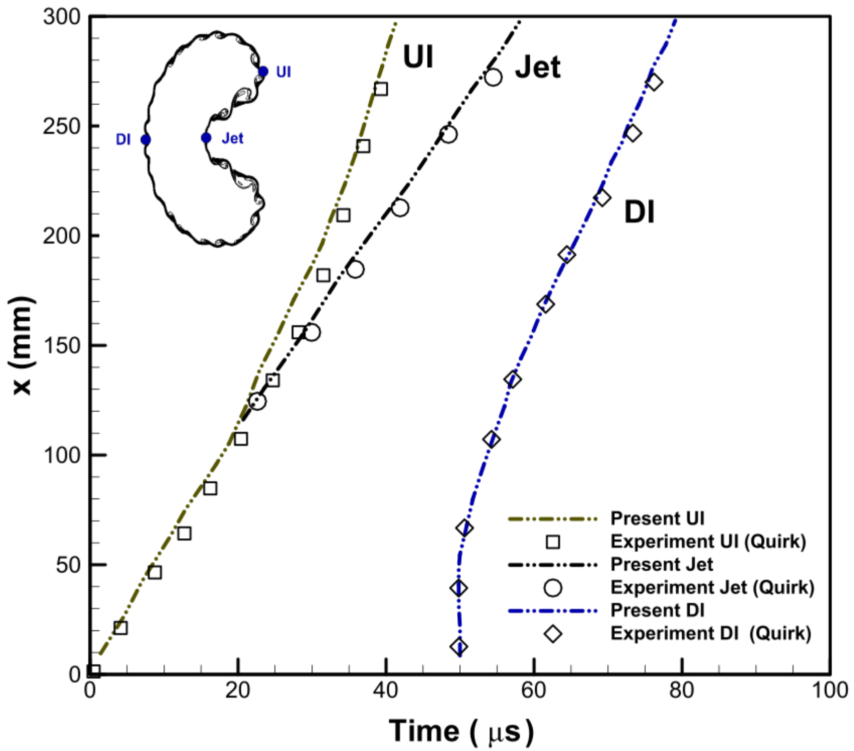


Characteristic interface points

Singh et al., Physics of Fluids, 33, 066103 (2021)

# 2D shock-cylindrical bubble interaction

**Experimental results (Ding et al., 2015)**

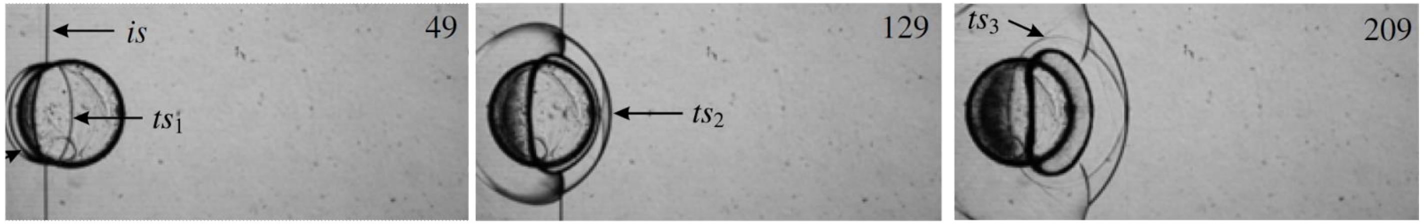


**Present results**

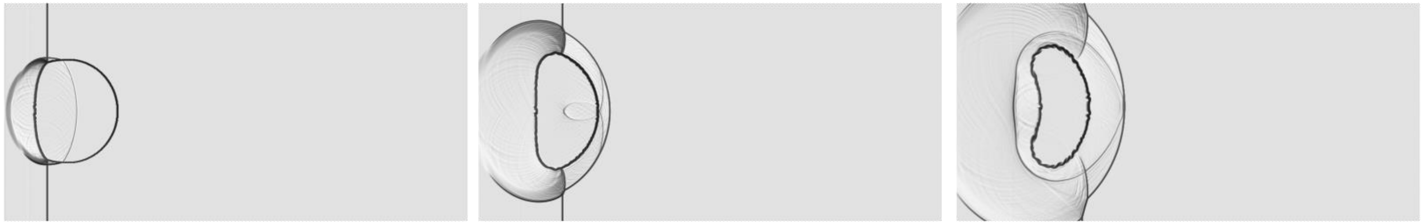

**Experimental results (Ding et al., 2015)**

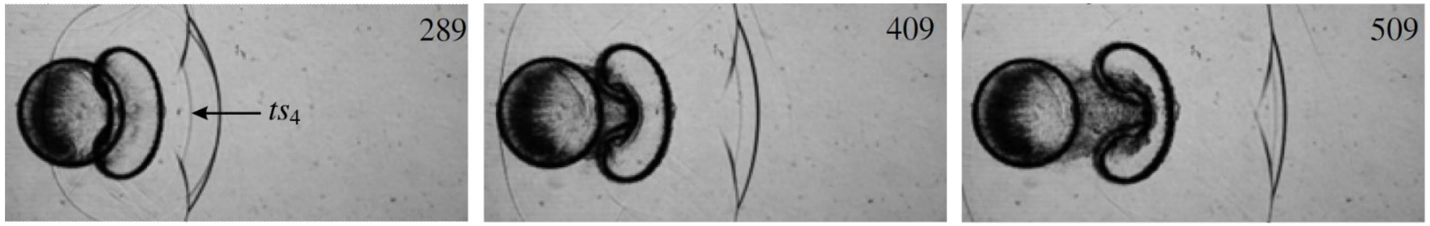


**Present results**

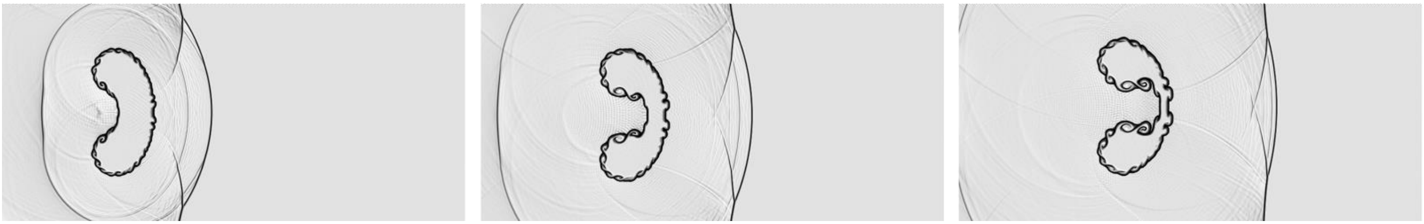

**Shock Mach number =1.29**
**Bubble filled with helium gas**

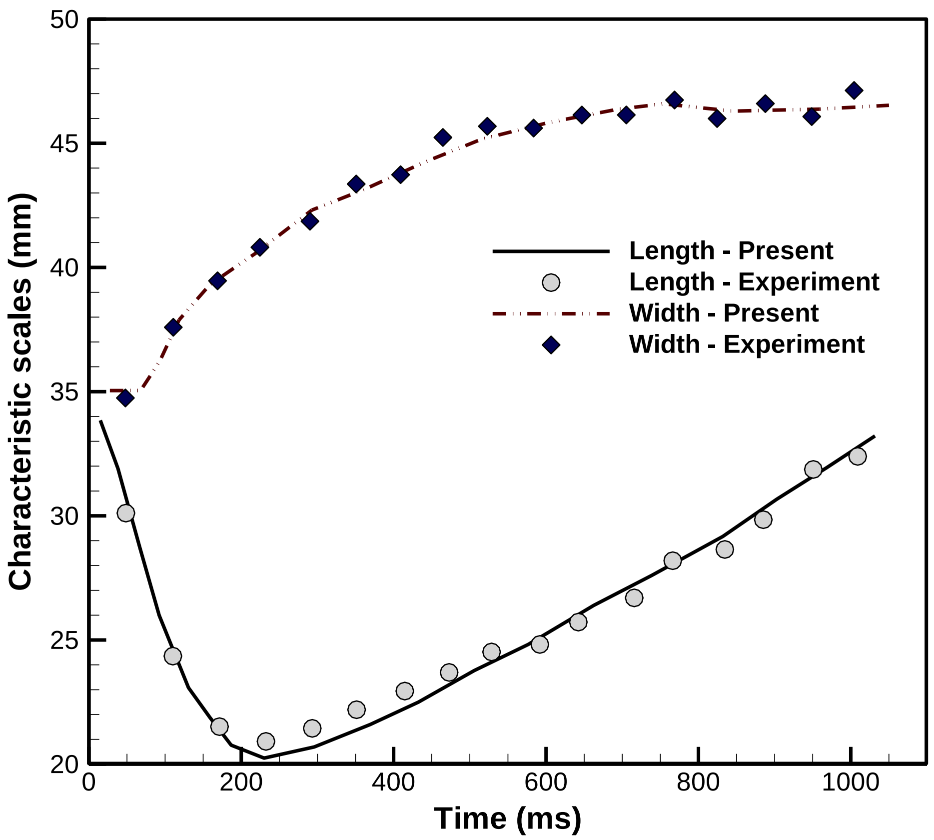


Singh, Physics of Fluids, 32, 126112 (2020)

Ding et al., J. Fluid Mech. 828, 289 (2017).

# 2D shock-square heavy bubble interaction

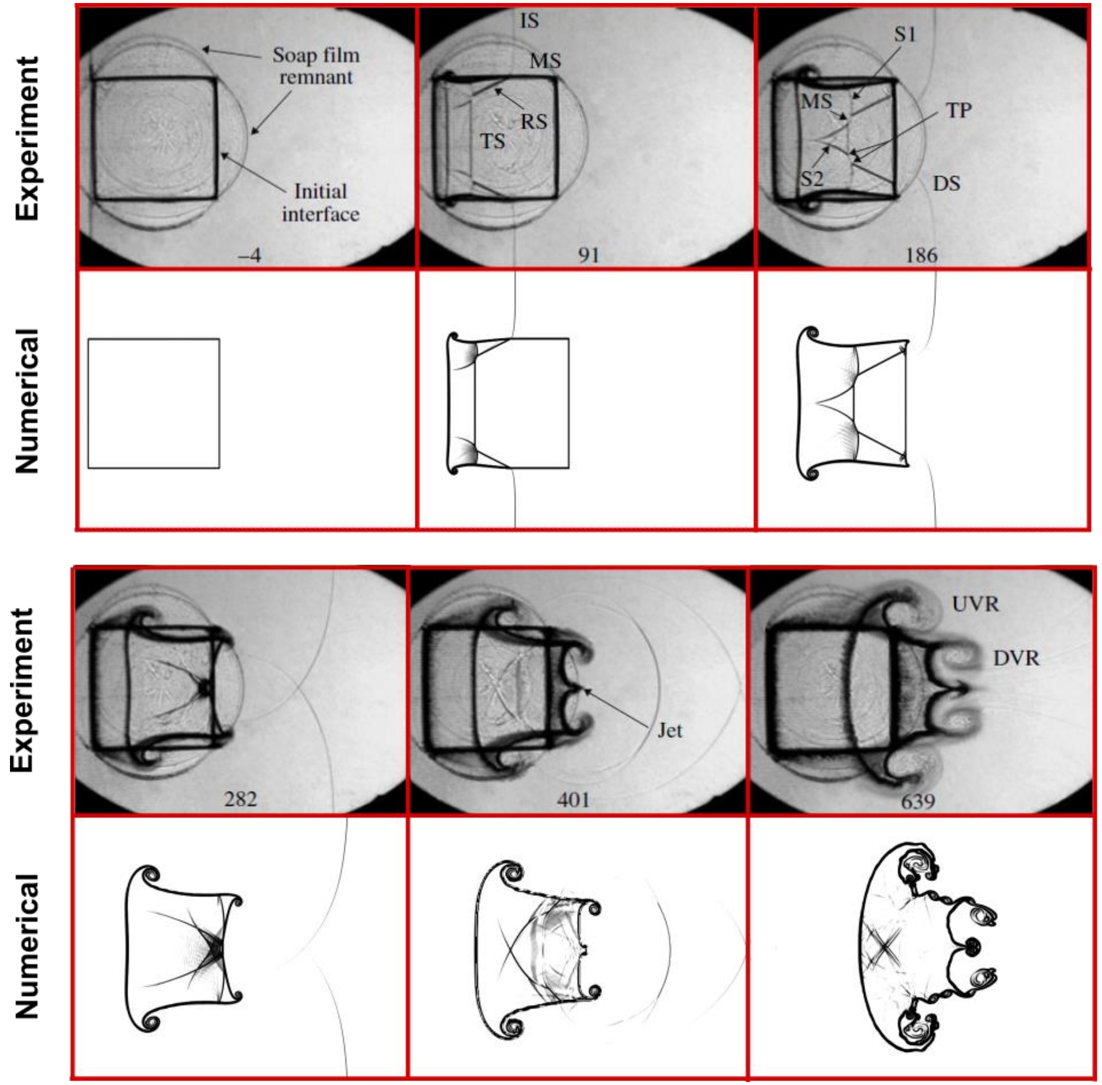


Numerical schlieren images

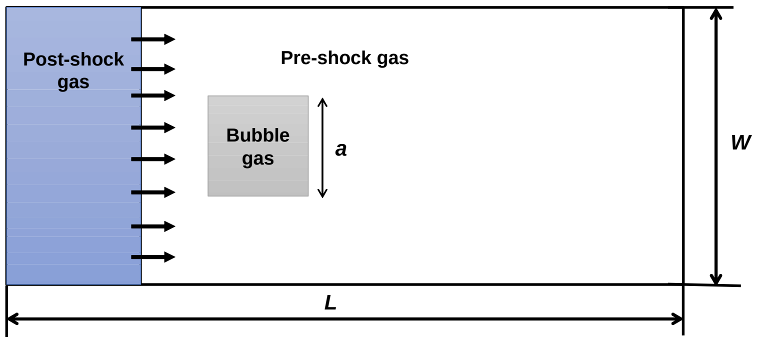


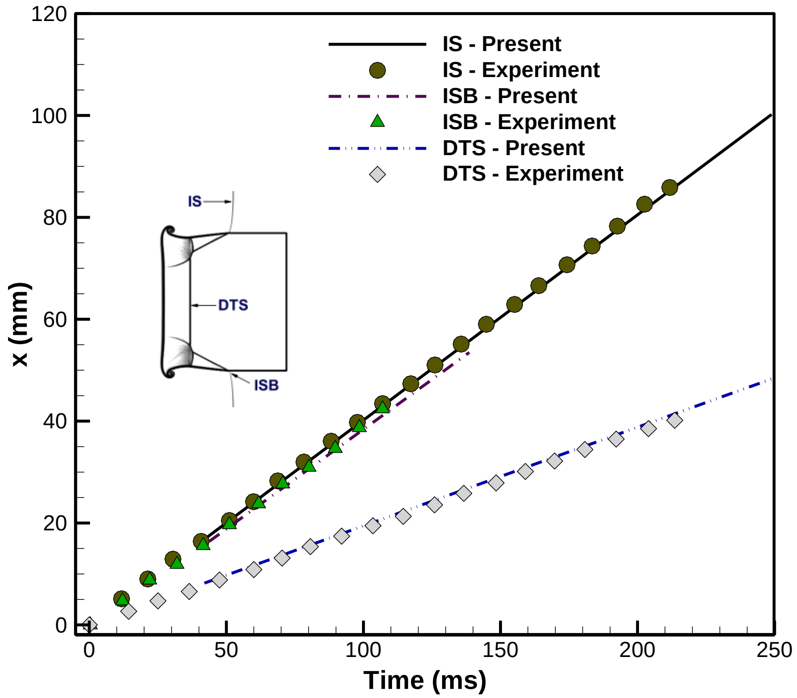


Shock trajectories points

Singh, Physics of Fluids, 32, 126112 (2020)

Luo et al., J. Fluid Mech. 773, 366–394 (2015)

# Flow morphology of shock-induced light square bubble

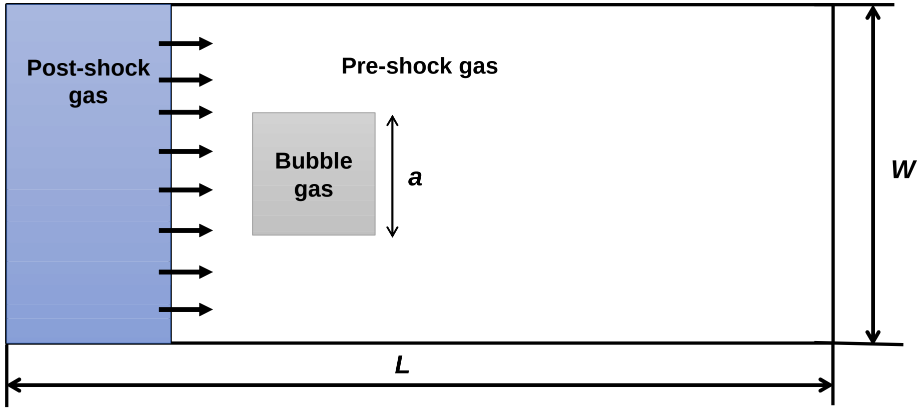


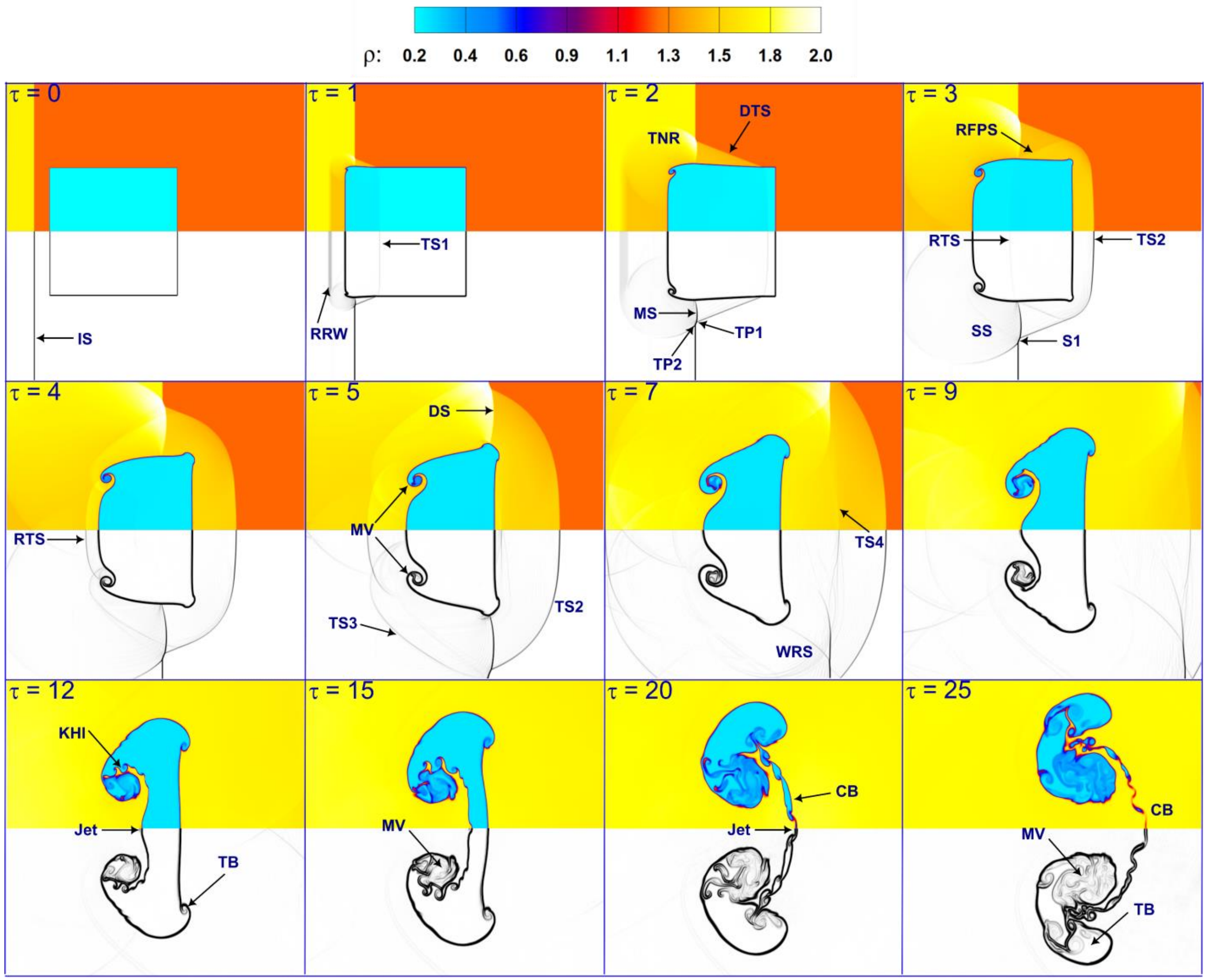


- ✓ Shock Mach number =1.21
- ✓ Bubble filled with helium gas
- ✓ Rankine-Hugoniot condition for initialization
- ✓ Third-order DG method
- ✓ Mesh of 1200x600 grid points

Singh and Torrilhon, Physics of Fluids, 35, 012117 (2023)

# Flow morphology of shock-induced heavy square bubble

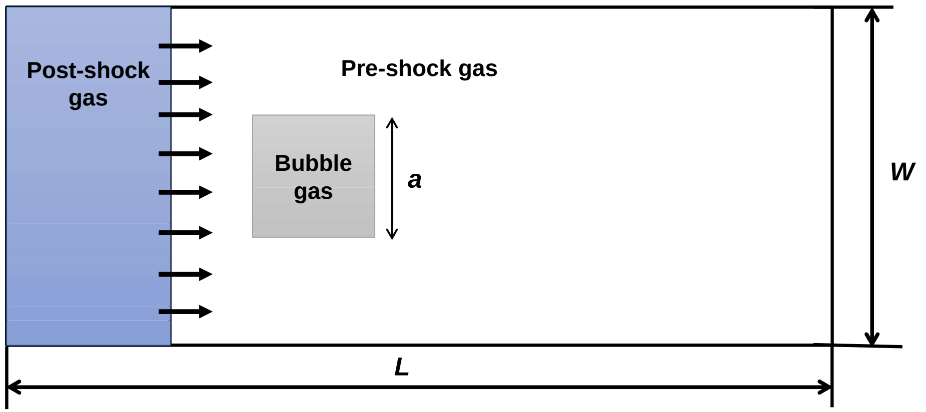


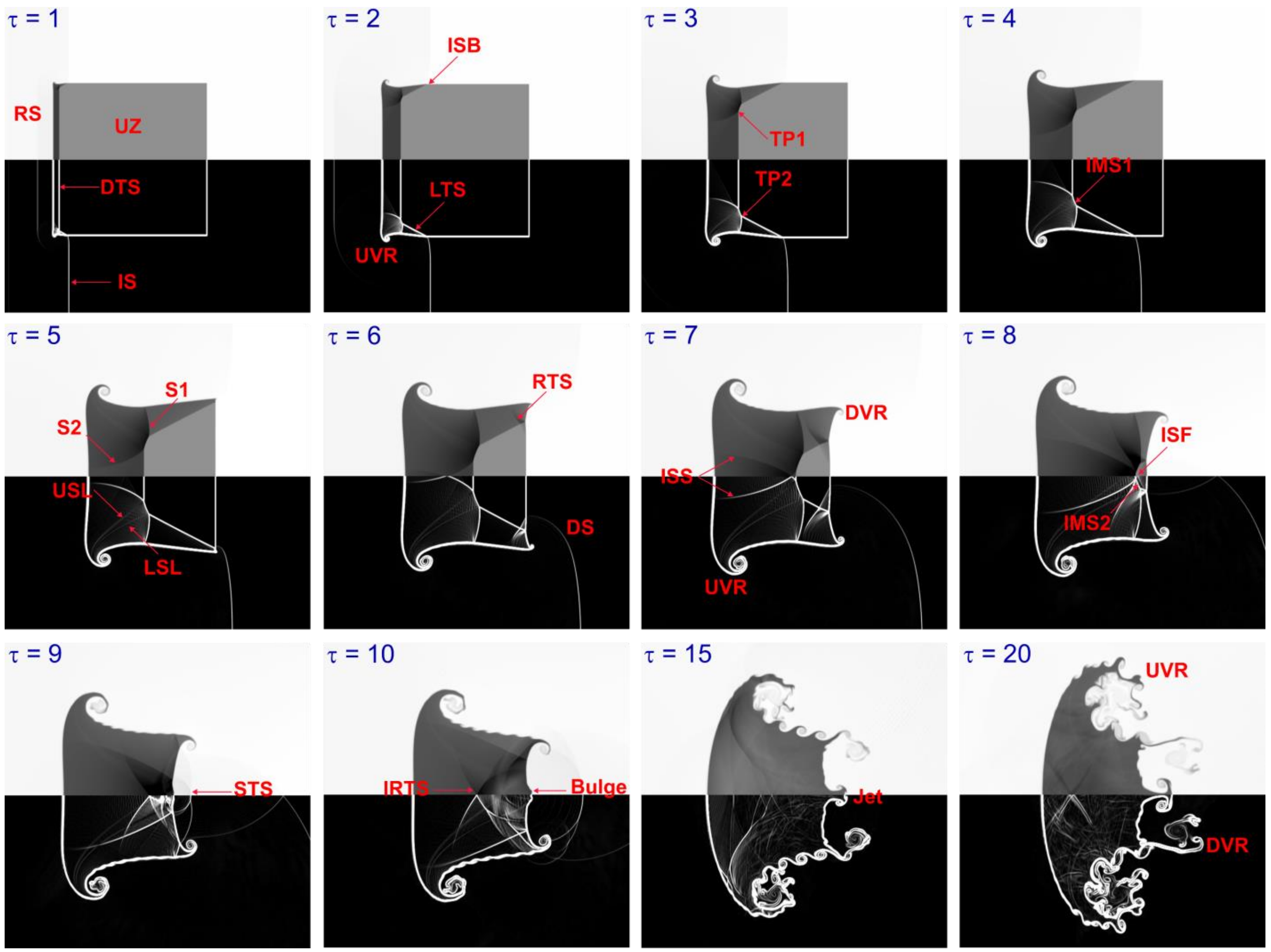


- ✓ Shock Mach number =1.21
- ✓ Bubble filled with SF6 gas
- ✓ Rankine-Hugoniot condition for initialization
- ✓ Third-order DG method
- ✓ Mesh of 1200x600 grid points

Singh and Battiato, Computer & Fluids, 242, 105502 (2022)

# Flow parameters on shock-induced hydrodynamics instability

- ✓ **Atwood number**
- ✓ **Bubble (interface) shape**
- ✓ **Incident shock Mach number**

**Atwood number is defined by**

$$\mathrm{At} = \frac{\rho_b - \rho_g}{\rho_b + \rho_g}$$

$\rho_b$ = bubble gas density

$\rho_g$ = ambient gas density

$\mathrm{At} > 0$: convergent configuration (light-heavy-configuration)

$\mathrm{At} < 0$: divergent configuration (heavy-light-configuration)

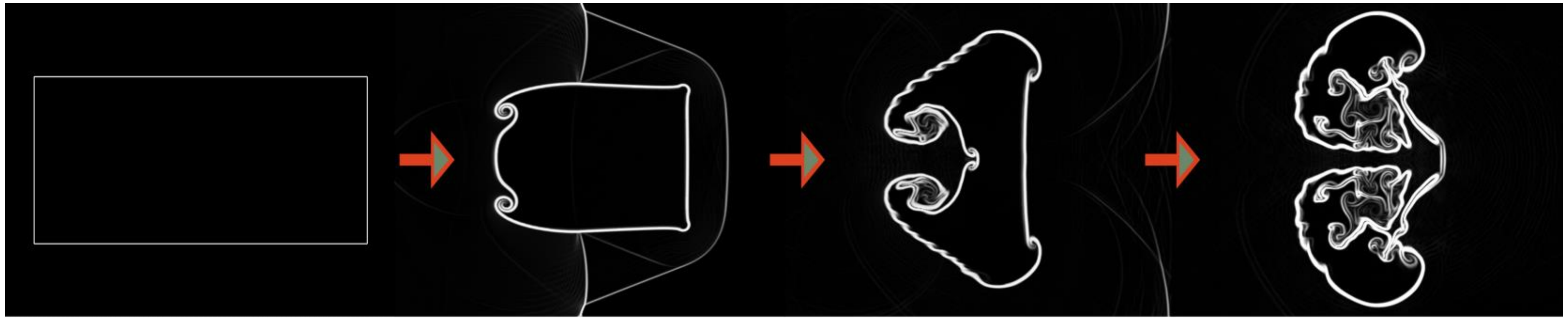

**(a) Light interface**

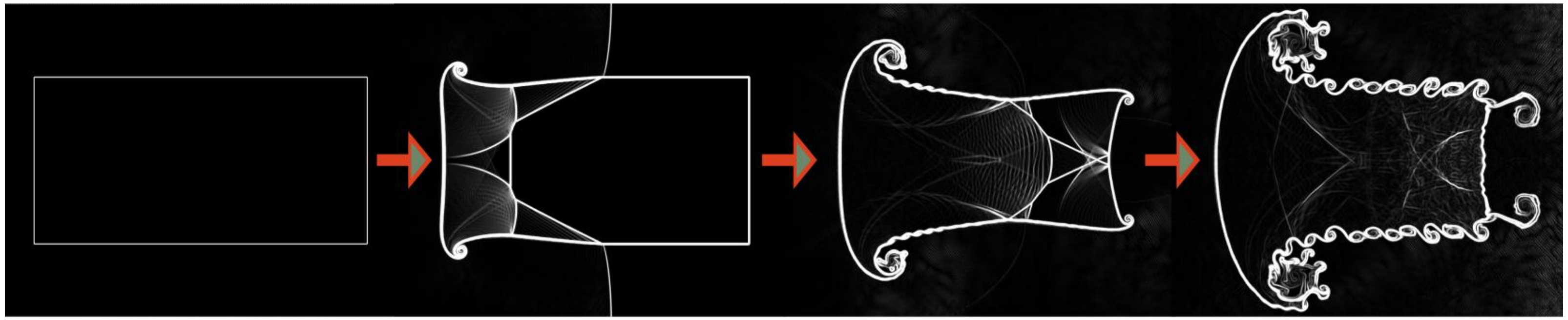

**(b) Heavy interface**

# Atwood number effects on shock-induced square bubble

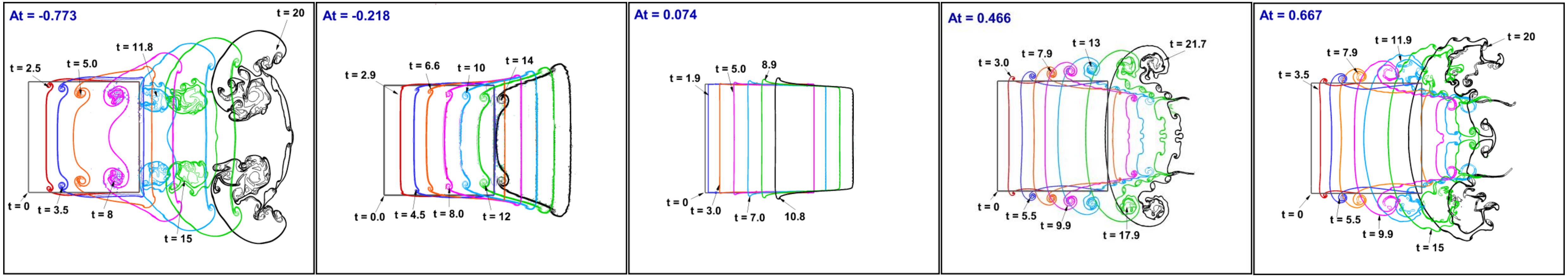


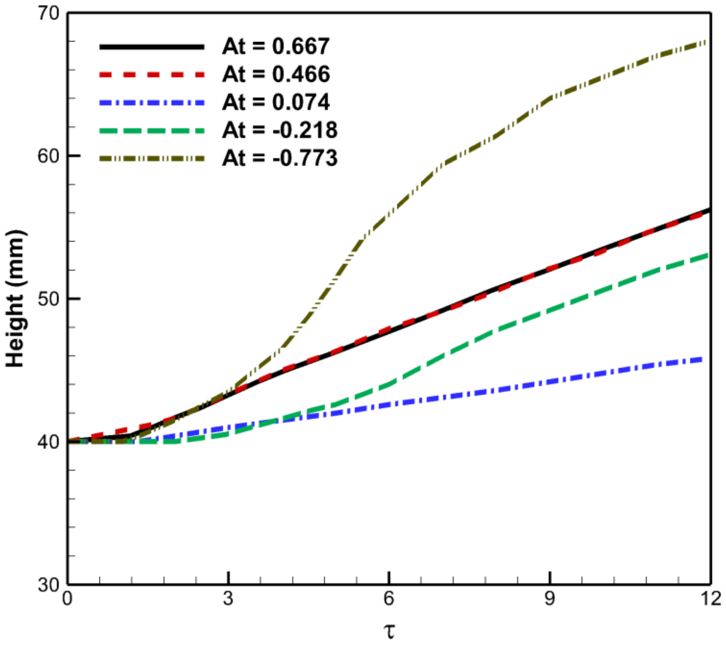


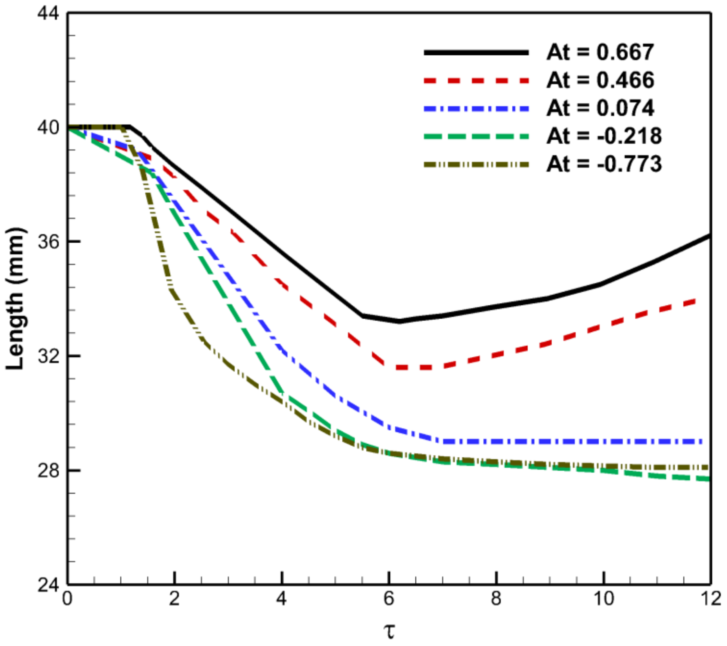


Singh, Physics of Fluids, 32, 126112 (2020)

# Interface shape effects on shock-induced bubble

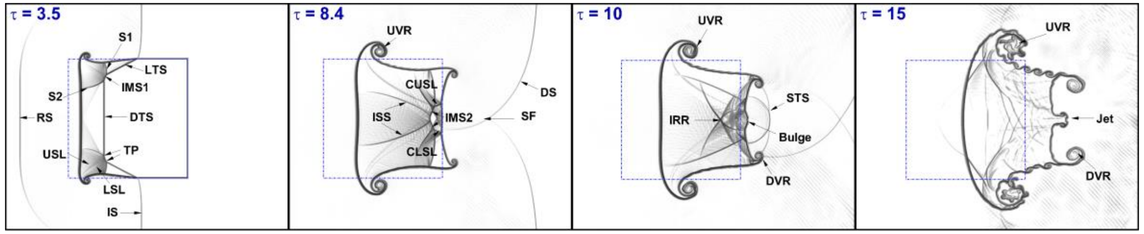


(a) Shock-accelerated $SF_6$ square bubble

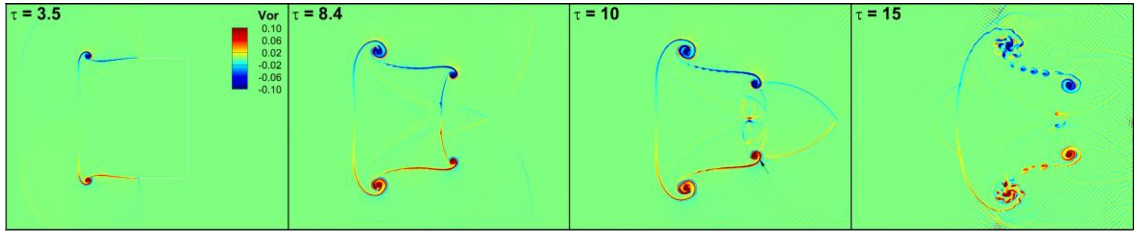


(a) Shock-accelerated $SF_6$ square bubble

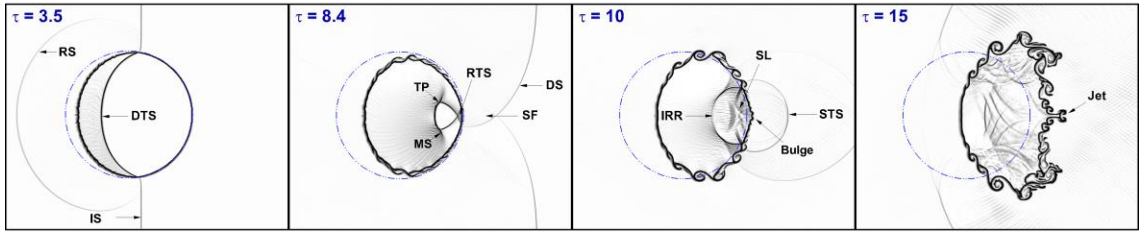


(b) Shock-accelerated $SF_6$ cylindrical bubble

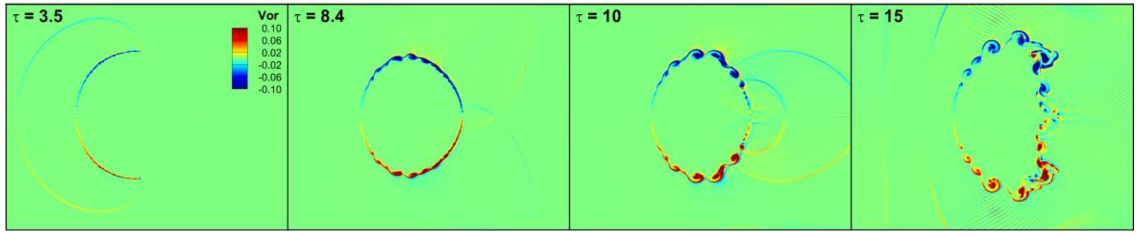


(b) Shock-accelerated $SF_6$ cylindrical bubble

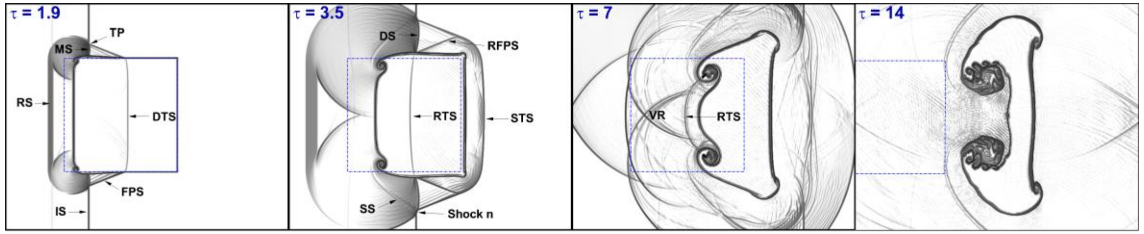


(a) Shock-accelerated He square bubble

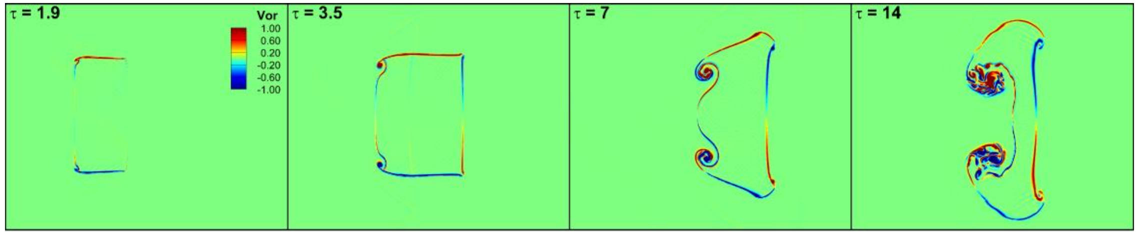


(a) Shock-accelerated He square bubble

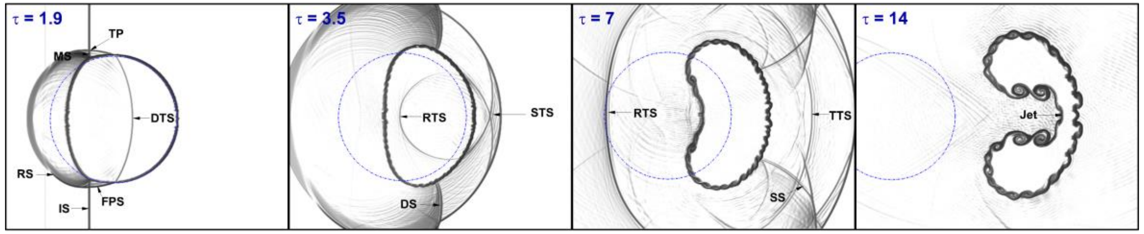


(b) Shock-accelerated He cylindrical bubble

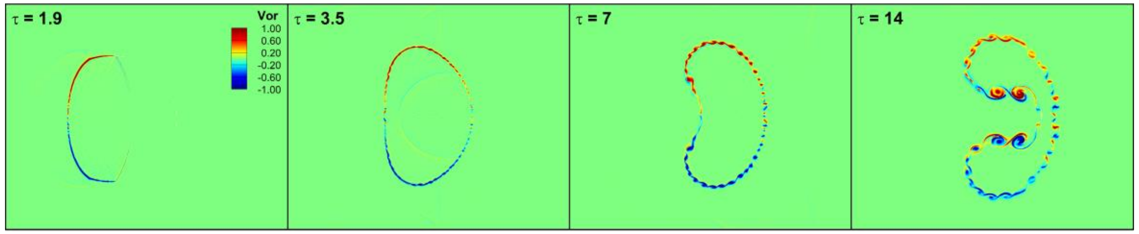


(b) Shock-accelerated He cylindrical bubble



Singh, Physics of Fluids, 32, 126112 (2020)

# Shock Mach number effects on shock-induced heavy square bubble

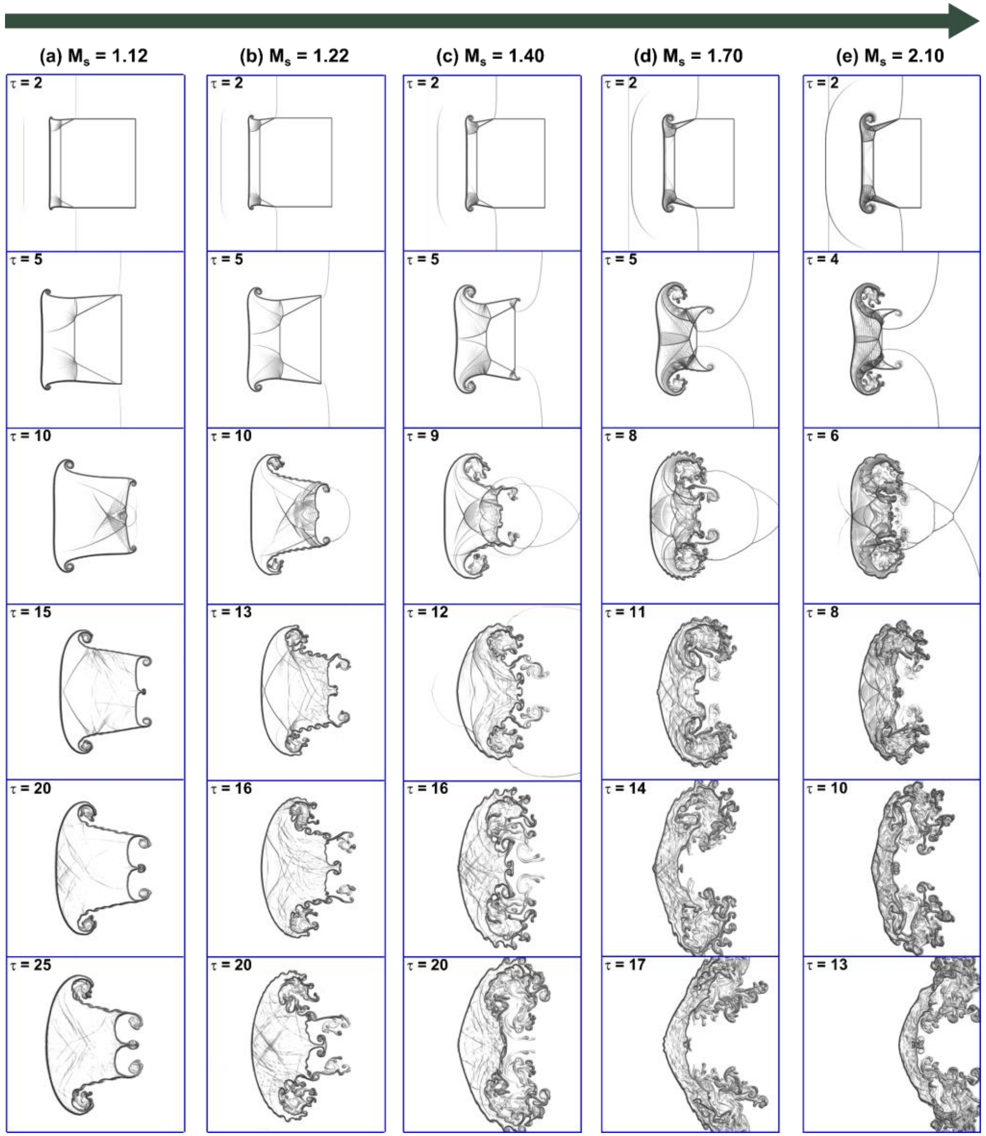


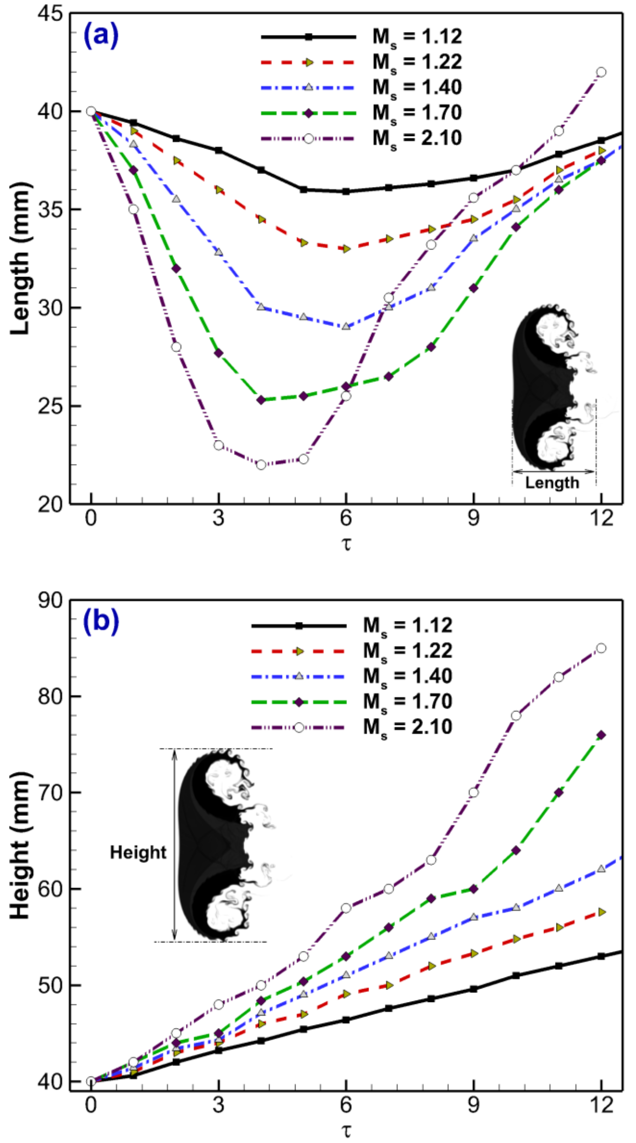


Singh and Battiato, accepted in Physica D: Nonlinear Phenomena (2023)

# Thermal non-equilibrium effects of diatomic and polyatomic gases

- ✓ Incident shock Mach number = 1.22
- ✓ Square helium gas bubble
- ✓ Ambient gases – argon, nitrogen, methane

$$\text{Dissipation Rate } (\varepsilon) = -\left[\left(\Pi_{xx} + f_b\Delta\right)S_{xx} + 2\Pi_{xy}S_{xy} + \left(\Pi_{yy} + f_b\Delta\right)S_{yy}\right]$$

$$S_{ij} = \frac{1}{2}\left(\frac{\partial u_i}{\partial u_j} + \frac{\partial u_j}{\partial u_i}\right)$$

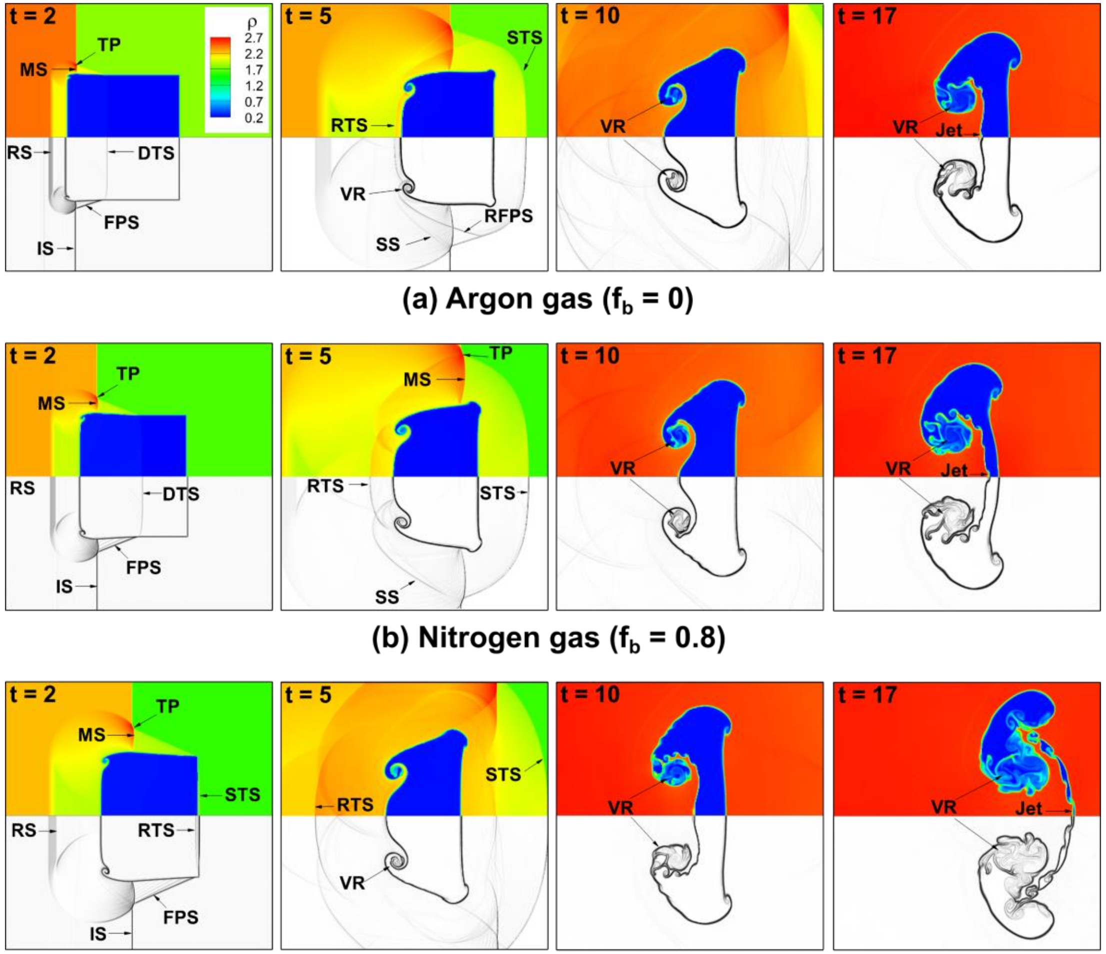

(a) Argon gas ($f_b$ = 0)

(b) Nitrogen gas ($f_b$ = 0.8)

(c) Methane gas ($f_b$ = 1.33)

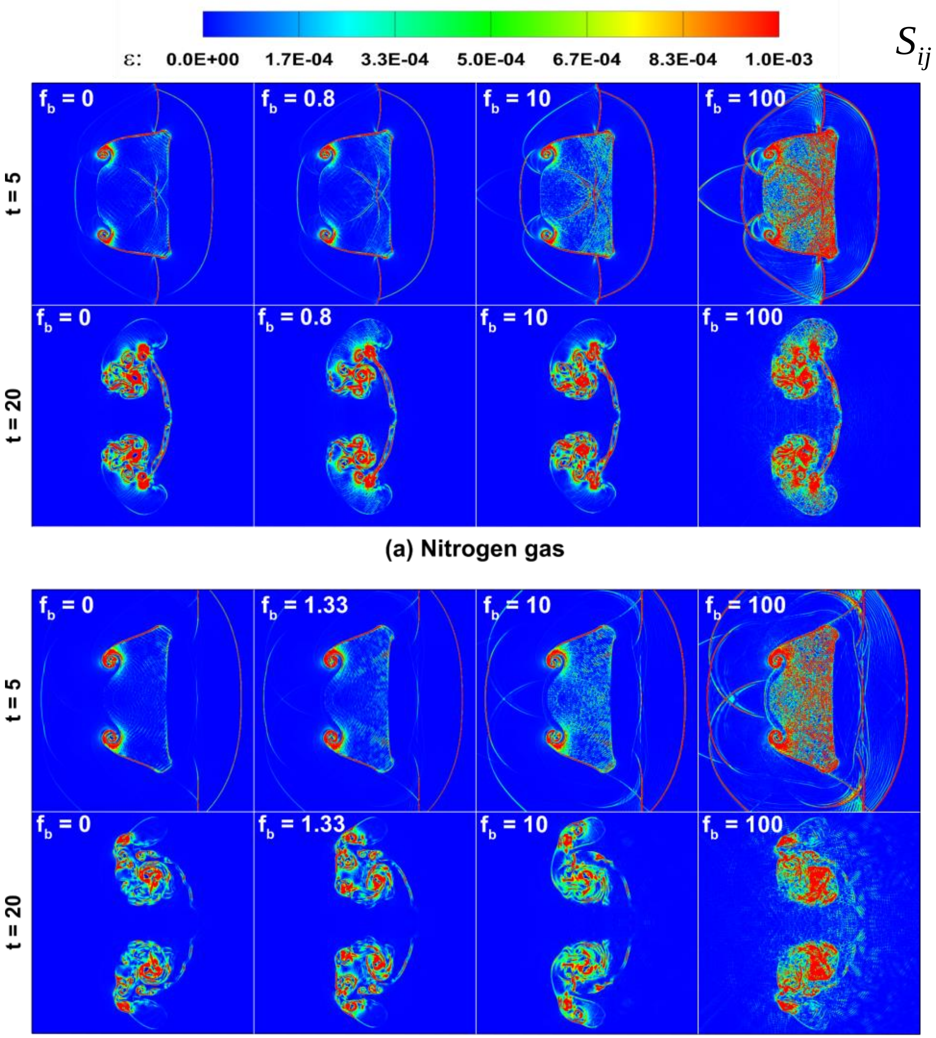

(a) Nitrogen gas

(b) Methane gas

**Singh, International Journal of Heat and Mass Transfer 179 , 121708 (2021)**

# Degree of thermal non-equilibrium

- In irreversible thermodynamics theory, the **degree of thermal nonequilibrium based on Rayleigh–Onsager theory** is a vital component and is directly related to entropy production in nonequilibrium processes.
- To demonstrate the degree of thermal nonequilibrium, the Rayleigh–Onsager dissipation function is defined as follows

$$R^* = \frac{\gamma M}{\mathrm{Re}} \frac{1}{p^*} \left[ \Pi^* : \Pi^* + 2\gamma' f_b \Delta^{*2} + \frac{2}{Ec \Pr} \frac{\mathrm{Q}^* \cdot \mathrm{Q}^*}{T^*} \right]^{1/2}$$

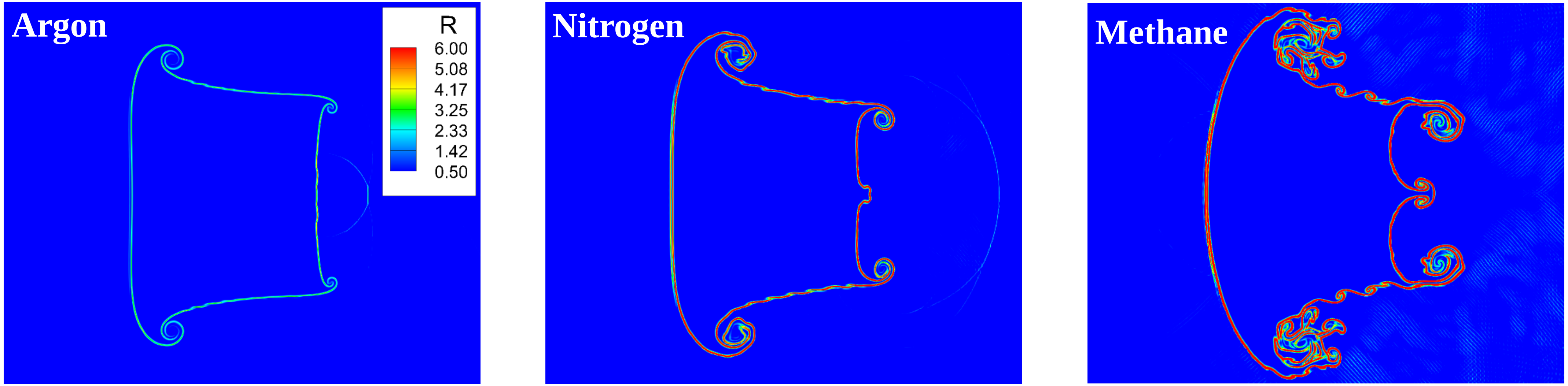


- The degree of nonequilibrium is **much higher** for diatomic and polyatomic gases than for monatomic gases.

# Effect of bulk viscosity ratio

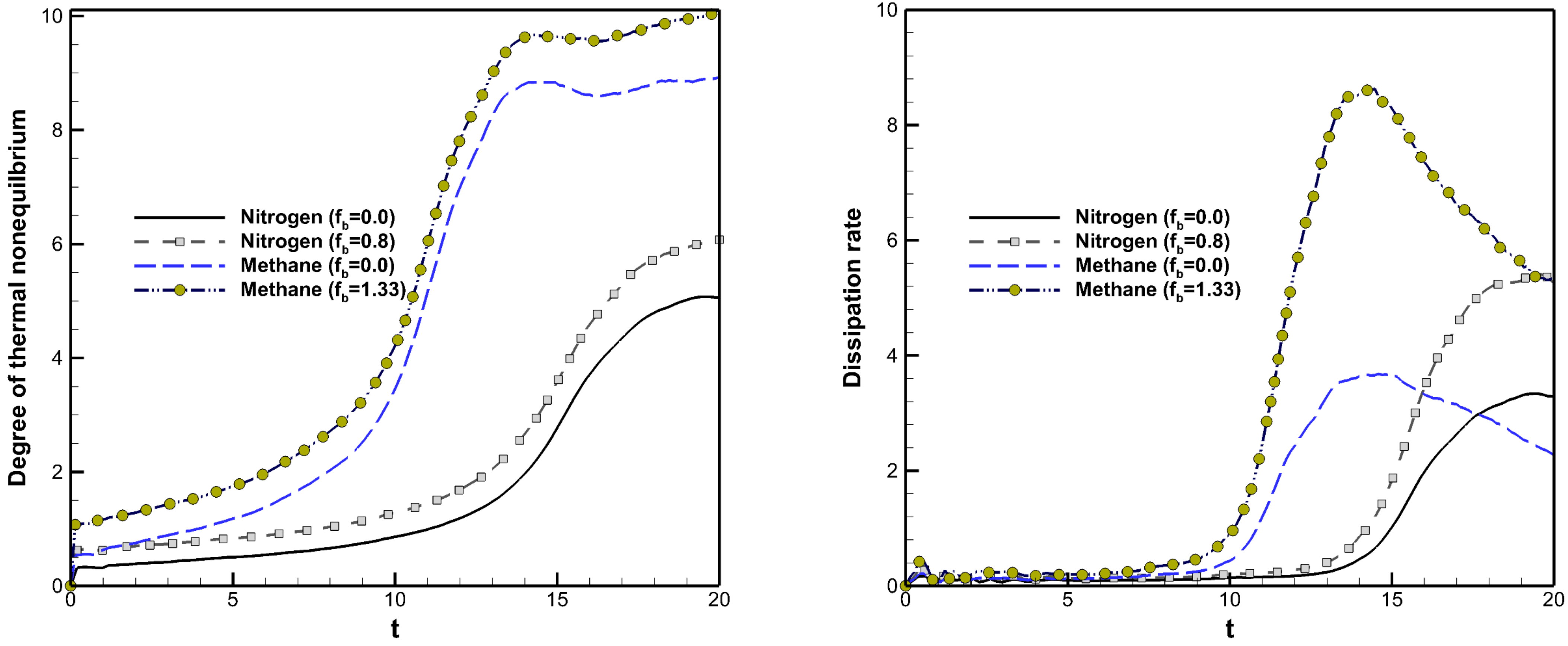


**Spatially integrated values of degree of thermal non-equilibrium and dissipation rate**

# Aspect ratio effects on shock-induced rectangular bubbles

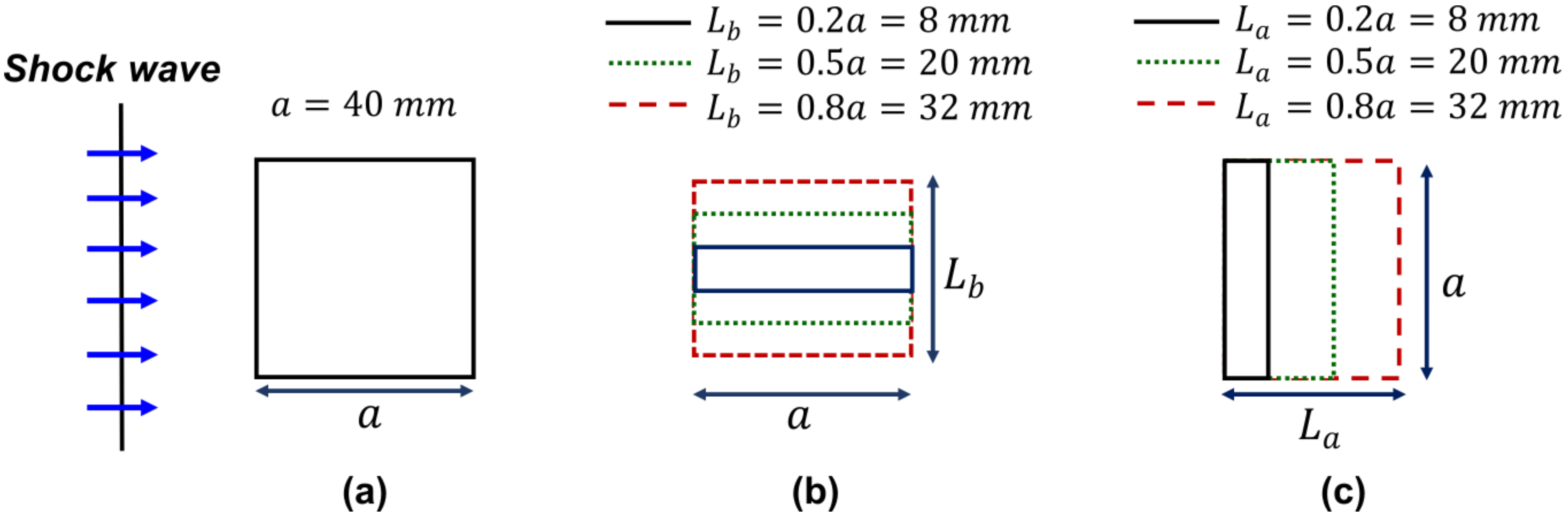


| Type of bubble | Case | $L_a$ | $L_b$ | Aspect ratio |
|---|---|---|---|---|
| Square | I | $a$ | $a$ | $AR_s = 1.0$ |
| Horizontal-aligned rectangular | II | $a$ | $0.8a$ | $AR_h = 1.25$ |
| | III | $a$ | $0.5a$ | $AR_h = 2.0$ |
| | IV | $a$ | $0.2a$ | $AR_h = 5.0$ |
| Vertical-aligned rectangular | V | $0.8a$ | $a$ | $AR_v = 1.25$ |
| | VI | $0.5a$ | $a$ | $AR_v = 2.0$ |
| | VII | $0.2a$ | $a$ | $AR_v = 5.0$ |

# Aspect ratio effects on shock-induced rectangular bubbles

Horizontal-aligned rectangular bubbles

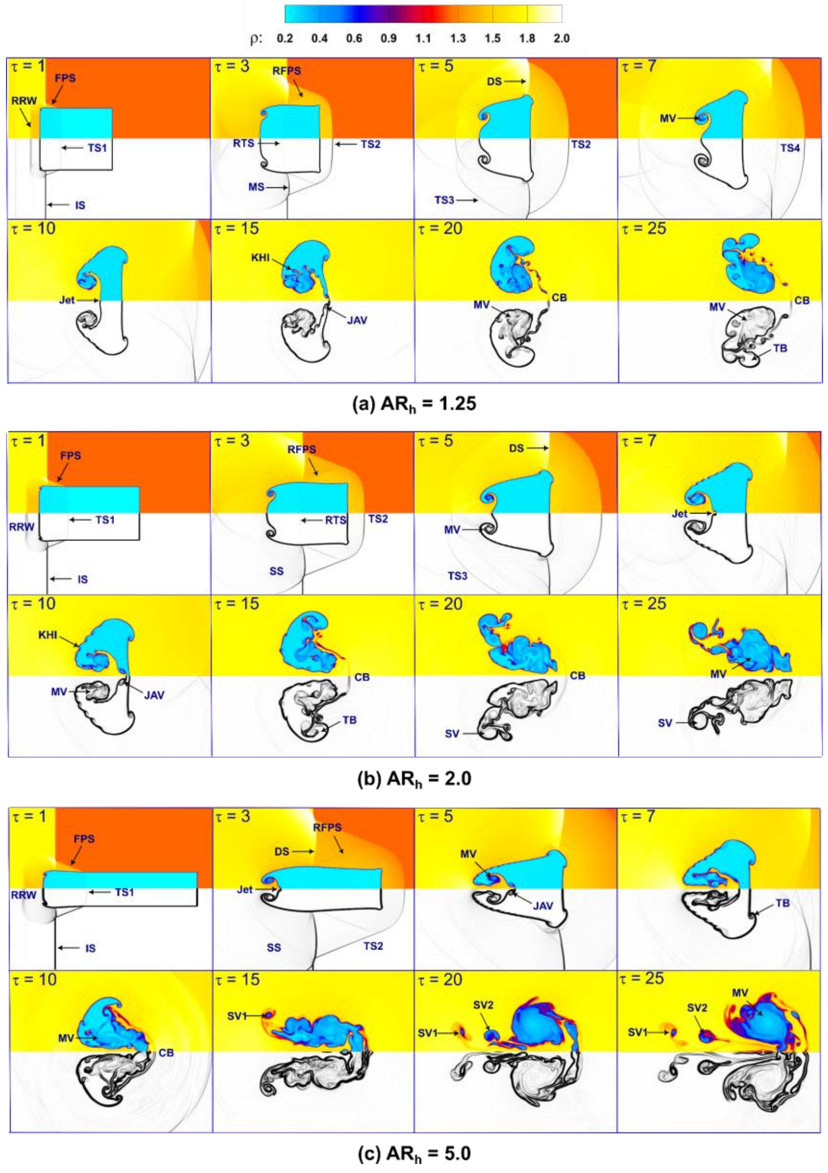

Vertical-aligned rectangular bubbles

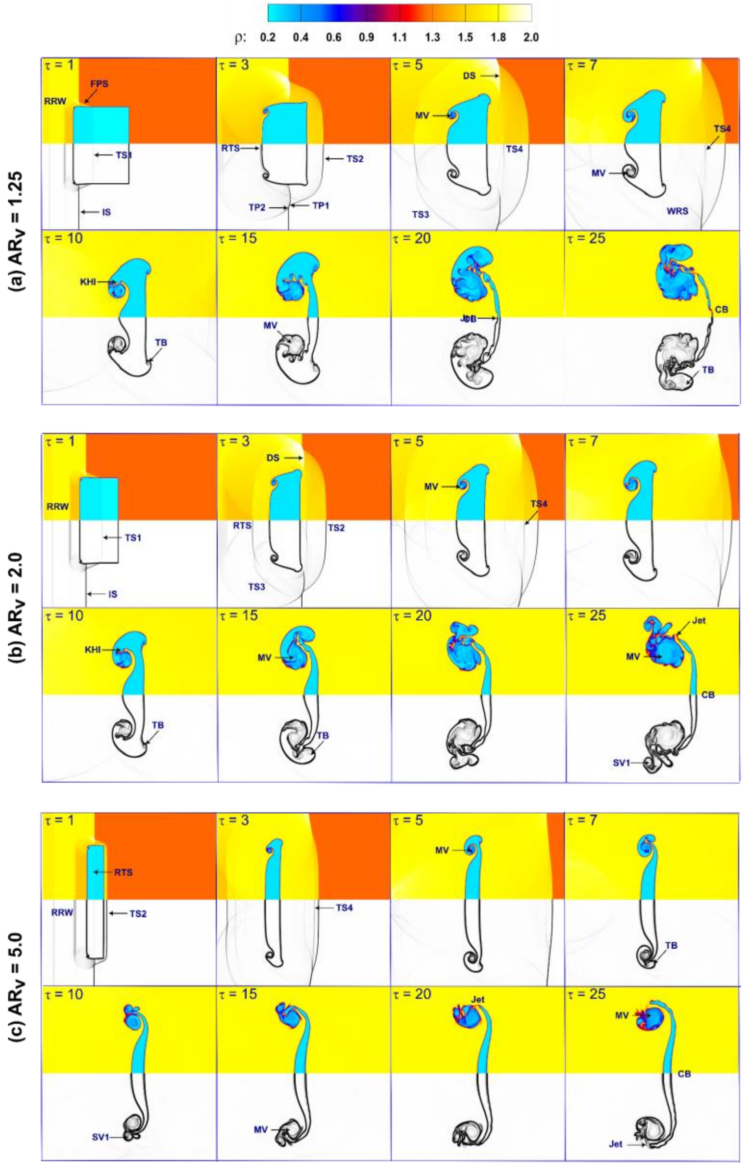



Singh and Torrilhon, Physics of Fluids, 35, 012117 (2023)

# Concluding remarks and future study

- The flow physics for shock-induced hydrodynamic instabilities on various gas bubbles with different shapes is investigated numerically.
- High fidelity simulations are performed with inhouse discontinuous Galerkin solver based on rectangular meshes
- Numerical results are validated with the existing experimental and computational results.
- Effects of various flow parameters – Shock Mach number, Atwood number, bubble shapes, thermal non-equilibrium – on the shock-induced bubbles are investigated.
- This study will be extended for shock-gas-liquid interaction-based problems.
- Reactive shock-induced hydrodynamic instabilities will be investigated with the applications of combustion and flame.

# Selected Articles on shock-induced hydrodynamic instabilities

- **S. Singh**, M. Torrilhon (2023), “On the shock-driven hydrodynamic instability in square and rectangular light gas bubbles: a comparative study from numerical simulations”, *Physics of Fluids*, 35, 012117 (2023)

- **S. Singh**, M. Battiato (2022), “Numerical simulations of Richtmyer-Meshkov instability of SF6 square bubble in diatomic and polyatomic gases”, *Computers & Fluids*, 242, 105502 (2022)

- **S. Singh** (2021), “Contribution of Mach number to the evolution of Richtmyer-Meshkov instability induced by a shock-accelerated square light bubble”, *Physical Review Fluids*, 6, 104001.

- **S. Singh** (2021), “Numerical investigation of thermal non-equilibrium effects of diatomic and polyatomic gases on the shock-accelerated light square bubble using a mixed-type modal discontinuous Galerkin method”, *International Journal of Heat and Mass Transfer*, 179, 121708

- **S. Singh**, M. Battiato, R. S. Myong (2021), “Impact of bulk viscosity on flow morphology of shock-accelerated cylindrical light bubble in diatomic and polyatomic gases”, *Physics of Fluids*, 33, 066103

- **S. Singh**, M. Battiato (2021), “Behavior of a shock-accelerated heavy cylindrical bubble under non-equilibrium conditions of diatomic and polyatomic gases”, *Physical Review Fluids*, 6, 044001

- **S. Singh** (2020), “Role of Atwood number on flow morphology of a planar shock-accelerated square bubble: A numerical study”, *Physics of Fluids*, 32, 126112

**If you are interested in my research work, you may visit/write me:**

https://www.researchgate.net/profile/Satyvir_Singh
https://www.acom.rwth-aachen.de/5people/singh/start
https://scholar.google.com.sg/citations?user=sQT89LYAAAAJ&hl=en

singh@acom.rwth-aachen.de
satyviriitm@gmail.com